MASTER'S THESIS

DIPLOMARBEIT

A NOVEL EXPERIMENTAL TECHNIQUE FOR DETERMINATION OF THE PERMEABILITY OF CONCRETE SUBJECTED TO HIGH TEMPERATURE

Eine neuartige Versuchseinrichtung zur Bestimmung der Permeabilität von Beton, der einer hohen Temperaturbelastung ausgesetzt war

ausgeführt zum Zwecke der Erlangung des akademischen Grades eines Diplom-Ingenieurs am

Institut für Mechanik der Werkstoffe und Strukturen
der
Technischen Universität Wien

unter Anleitung von

Dipl.-Ing. **Matthias Zeiml**
und
Univ.-Doz. Dipl.-Ing. Dr.techn. **Roman Lackner**

durch

Georg FERNER

E 610 / 99 26 463
Kuefsteingasse 42
A-1140 Wien

Wien, im Mai 2005

Danksagung

An dieser Stelle möchte ich mich bei all jenen bedanken, die zum Zustandekommen dieser Arbeit beigetragen haben.

Besonderer Dank sei meinen Eltern ausgesprochen, welche mir das Studium ermöglicht haben und mich immer mit Rat und Tat unterstützt haben.

Herrn Univ.Doz. Dipl.-Ing. Dr. techn. Roman Lackner gebührt Dank für die reibungslose Betreuung dieser Arbeit, welche sogar trotz seines Aufenthaltes am MIT, Cambridge sehr gut funktioniert hat.

Bei Herrn Dipl.-Ing. Matthias Zeiml möchte ich mich für die Hilfestellung bei der Versuchsdurchführung bedanken.

Weiters möchte ich mich auch bei den Mitarbeitern im Laboratorium des Institutes der Mechanik für Werkstoffe und Strukturen, insbesonders bei Herrn Wolfgang Dörner bedanken.

Für die Unterstützung bei der Durchführung der Versuchsreihen im Laboratorium des Institutes der Mechanik für Werkstoffe und Strukturen, Abteilung Baustoffforschung möchte ich mich bei Herrn Dipl.-Ing. Dr.techn. Martin Fleischmann und Herrn Dr.Phil Roland Reihsner bedanken.

Dank gebührt Herrn o.Univ.Prof. Dipl.-Ing. Dr.techn. Ulrich Schneider und Herrn Dipl.-Ing. Hadubrand Harand vom Institut für Hochbau und Technologie (Zentrum für Baustofforschung, Werkstofftechnik und Brandschutz) für die Unterstüzung bei der Herstellung der Probekörper, Hilfestellung bei den Temperaturversuchen und die hervorragende Zusammenarbeit.

Dank gilt auch all jenen Personen, die mir, in welcher Form auch immer, hilfreich zur Seite standen, hier jedoch nicht namentlich erwähnt wurden.

Ich danke besonders meiner Freundin Magdalena Lindemayr, dass sie mich immer wieder mit ihrer guten Laune begleitet hat.

Wien, im Mai 2005 Georg FERNER

Summary

Recent tunnel fires and the increasing demand for the safety assessment of tunnels under fire lead to the improvement of lining concrete with respect to its performance at high temperatures. Hereby, special attention was paid to the phenomenon of explosive spalling of near-surface concrete layers.

At high temperatures, the evaporation of physically and chemically bound water results in an increase of vapor pressure in the pore system. When the vapor pressure in the concrete is not sufficiently reduced by vapor transport towards the heated surface, spalling may occur.

Several investigations claim that the allowance of polypropylene fibers (PP-fibers) to the mix design of concrete improves the high-temperature performance of concrete. PP-fibers melt at approximately 160 °C and leave channels for the water vapor to escape.

In this thesis, the permeability of concrete with and without PP-fibers subjected to high temperatures is investigated. For this purpose, an experimental device recently developed at the Institute for Mechanics of Materials and Structures at Vienna University of Technology was improved, allowing now conduction of two types of experiments: decreasing-pressure and constant-pressure experiments. By employing a newly-developed search algorithm, the intrinsic permeability and the parameter, accounting for the pressure dependence of the apparent permeability, are determined.

Kurzfassung

In den vergangenen Jahren haben Tunnelbrände und das Bedürfnis nach mehr Sicherheit in Tunnels zu einer Verbesserung des Innenschalenbetons in Hinblick auf sein Verhalten im Brandfall geführt. Ein besonderes Augenmerk wurde dabei auf das explosionsartige Abplatzen von oberflächennahen Betonschichten gelegt.

Bei hohen Temperaturen kommt es infolge Verdampfens von chemisch und physikalisch gebundenen Wassers in Beton zu einem Druckaufbau, welcher, wenn er nicht genügend rasch durch den Transport zur beflammten Betonoberfläche abgebaut werden kann, zu den zuvor erwähnten explosionsartigen Abplatzungen führen kann.

Im Rahmen von Untersuchungen über die Temperaturbelastbarkeit von Beton wurde die Zugabe von Polypropylenfasern (PP-Fasern) zum Beton als wirkungsvolles Mittel zur Vermeidung von Abplatzungen festgestellt. PP-Fasern schmelzen bei einer Temperatur von ungefähr 160 °C und hinterlassen Kanäle, in denen der Wasserdampf entweichen kann.

In dieser Arbeit wird die Permeabilität von Beton mit und ohne PP-Fasern, der einer Temperaturbelastung ausgesetzt wurde, experimentell untersucht. Zu diesem Zweck wurde eine auf dem Institut für Mechanik der Werkstoffe und Strukturen der Technischen Universität Wien entwickelte Versuchseinrichtung im Hinblick auf die Durchführung von Versuchen bei konstantem Druck verbessert. Mit der neuen Versuchseinrichtung konnten Permeabilitätsversuche mit konstantem und abfallendem Druck durchgeführt werden. Für die Auswertung der im Rahmen der Durchlässigkeitsuntersuchungen erhaltenen Messwerte kommt ein Suchalgorithmus zum Einsatz, der die sogenannte intrinsische Permeabilität und jenen Parameter, der die Druckabhängigkeit der Permeabilität berücksichtigt, liefert.

Contents

Chapter 1

Motivation

Recent tunnel fires and the damage of the lining observed after tunnel fires lead to an increasing concern regarding the safety of tunnel linings subjected to fire. Explosive spalling of near-surface layers, resulting from evaporation of pore water, leads to reduction of the cross-section of the lining which, in case of shallow tunnels, may result in collapse of the tunnel. In several publications, the beneficial effect of polypropylene fibers (PP-fibers) with respect to the spalling depth was reported. Hereby, melting of PP-fibers at approximately 160 °C leaves channels in which the water vapor is transported towards the heated surface. In this thesis, the increase of the permeability of concrete subjected to high temperatures is investigated. The theoretical basis, i.e., the underlying differential equation describing water-vapor transport and the two material parameters defining the permeability of concrete, is provided in Chapter 2. In Chapter 3, the experimental setup used for determination of these parameters is presented. This setup allows conduction of two types of tests, referred to as constant-pressure experiments (CPEs) and decreasing-pressure experiments (DPEs). The mix design of the concrete considered in this thesis, which was chosen similar to the one of the concrete investigated in previous experimental studies performed at the Institute for Mechanics of Materials and Structures at Vienna University of Technology, is described in Chapter 4. In Chapter 5, the results obtained from permeability tests performed in this thesis and results reported in (Leithner 2004) are presented. The discussion of these test results with respect to the reliability of the underlying test equipment and the used mode of determination of permeability parameters is given in Chapter 6. Finally, the temperature dependence of the permeability of concrete and concluding remarks are given in Chapter 7.

Chapter 2

Introduction

The transport through porous media such as concrete is defined by the viscosity of the fluid passing through the pore space and the pore space, i.e., the geometrical properties of the material microstructure. The latter is described by the size, shape, orientation, and distribution of pores. As regards the flow of gas through porous media, the water saturation, leaving less space for the gas flow, influences the transport properties (Gallé and Daian 2000; Jacobs 1994).
In case of the flow of water vapor towards the heated surface of concrete members subjected to fire load, the water saturation is zero as the temperature exceeds 100°C (dried conditions), whereas, both the pore space and the viscosity of the fluid change with increasing temperature.[1]
The flow of water vapor in heated concrete is described by Darcy's law, reading

$$q = k \frac{1}{\eta} \frac{d\,p}{d\,x}, \tag{2.1}$$

where q [$\mathrm{m}^3/(\mathrm{m}^2\ \ \mathrm{s})$] is the volumetric flux of water vapor, η [$\mathrm{N\,s/m}^2$] is the dynamic viscosity of water vapor, p [Pa] is the pressure, and k [m^2] is the apparent permeability. The latter is a function of the pressure, reading (Klinkenberg 1941)

$$k = k_{int} \left(1 + \frac{b}{p}\right), \tag{2.2}$$

where k_{int} [m^2] is referred to as intrinsic permeability, representing the geometrical properties of the pore space, and b [Pa] is a constant parameter (see Figure 2.1).

[1] According to Gawin et al. (2002), the viscosity of gas increases lineraly with temperature. The pore space of concrete increases with temperature in consequence of dehydration of concrete and microcracking (Leithner 2004).

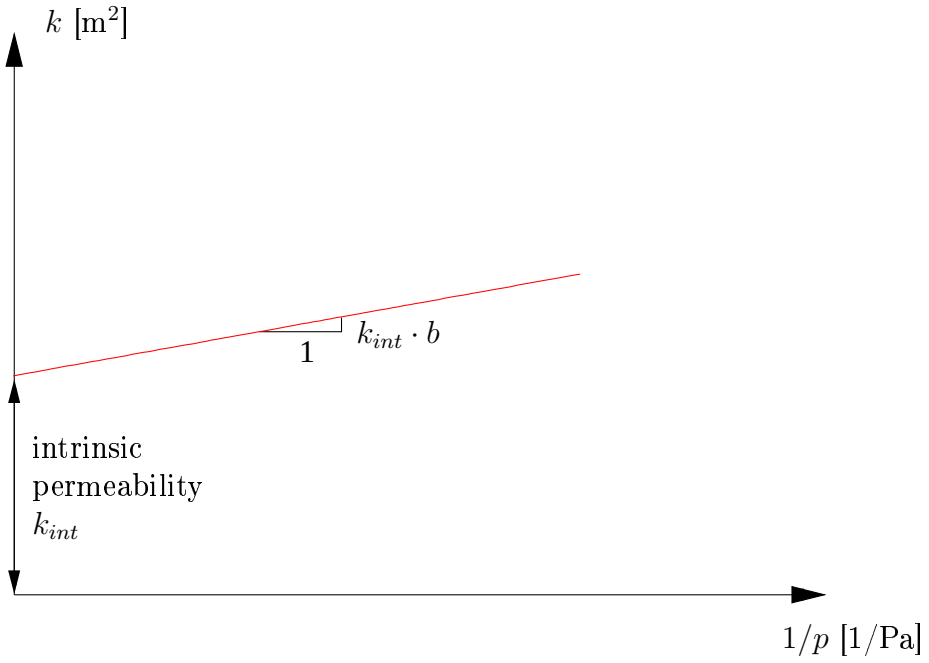

Figure 2.1: Dependence of the apparent permeability k on the pressure according to Klinkenberg (1941)

The determination of k_{int} and b for concrete pre-heated to different temperatures is the goal of this thesis, giving $k_{int}(T)$ and $b(T)$ and, via Equation (2.2), $k(T, p)$. The employed experimental setup and the mode of determining k_{int} and b from experimental data are presented in the following chapter.

Chapter 3

Methods

3.1 Experimental setup

In this work, the experimental setup described in (Leithner 2004) was improved, now allowing – in addition to decreasing-pressure experiments (DPEs) – conduction of so-called constant-pressure experiments (CPEs). The latter are essential in case of high permeabilities as observed for concrete heated up to 400°C and above. In the course of CPEs and DPEs, the air pressure p_t at the top surface of the cylindrical specimen (see Figure 3.1(a)) is increased, while the bottom surface is open to the atmospheric pressure, with $p_b = p_0$. The side surface of the specimen is sealed with wax. Thus, the difference in the air pressure induces a one-dimensional gas flow from the top to the bottom of the specimen. While the pressure p_t is held constant during CPEs, it decreases with time in the course of DPEs (see Figure 3.1(b)).

Constant-pressure experiments (CPEs)

In order to provide an (in-average) constant air pressure p_t for CPEs, two air-supplying pistons were considered (see Figures 3.2 and 3.3). The two pistons are powered by a double-acting piston located in between them. During movement in one direction, one piston is filled with air from the gas supply, while the air in the other piston is compressed and, as the pressure in the piston exceeds the pressure p_t of the test chamber, supplied to the test chamber. The flow of air is controlled by four one-way valves, which guarantee that the air flows only from the gas supply into the two pistons and, thereafter, towards the test chamber. These valves work properly as long as the pressure of the gas supply (filling pressure) is lower than the pressure p_t in the test chamber. The following quantities

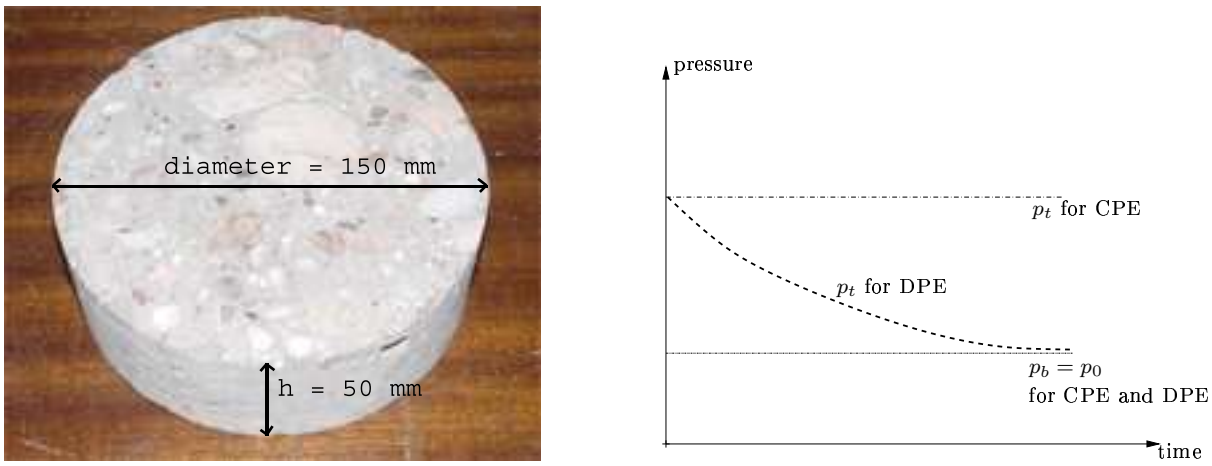

(a) (b)

Figure 3.1: (a) photo of test specimen and (b) illustration of pressure histories for CPEs and DPEs (p_t: pressure at the top surface of the specimen; p_b: atmospheric pressure at the bottom surface of the specimen)

are recorded during CPEs:

- pressure in the test chamber, $p_t(t)$,
- pressure in the pistons, $p_{p,1}(t)$ and $p_{p,2}(t)$, and
- movement of double-acting piston, $u(t)$.

Decreasing pressure experiments (DPEs)

During DPEs, the pressure p_t at the top surface of the cylindrical specimen decreases with time (see Figure 3.1). For these experiments, the same experimental setup used for the CPEs (Figures 3.2 and 3.3) was employed. However, the pressure pistons were disconnected and a container (volume = 20.8 l) was connected to the test chamber (see Figure 3.3). The decrease of pressure in the test-chamber – container system, resulting from flow of air through the specimen, is recorded by $p_t(t)$.

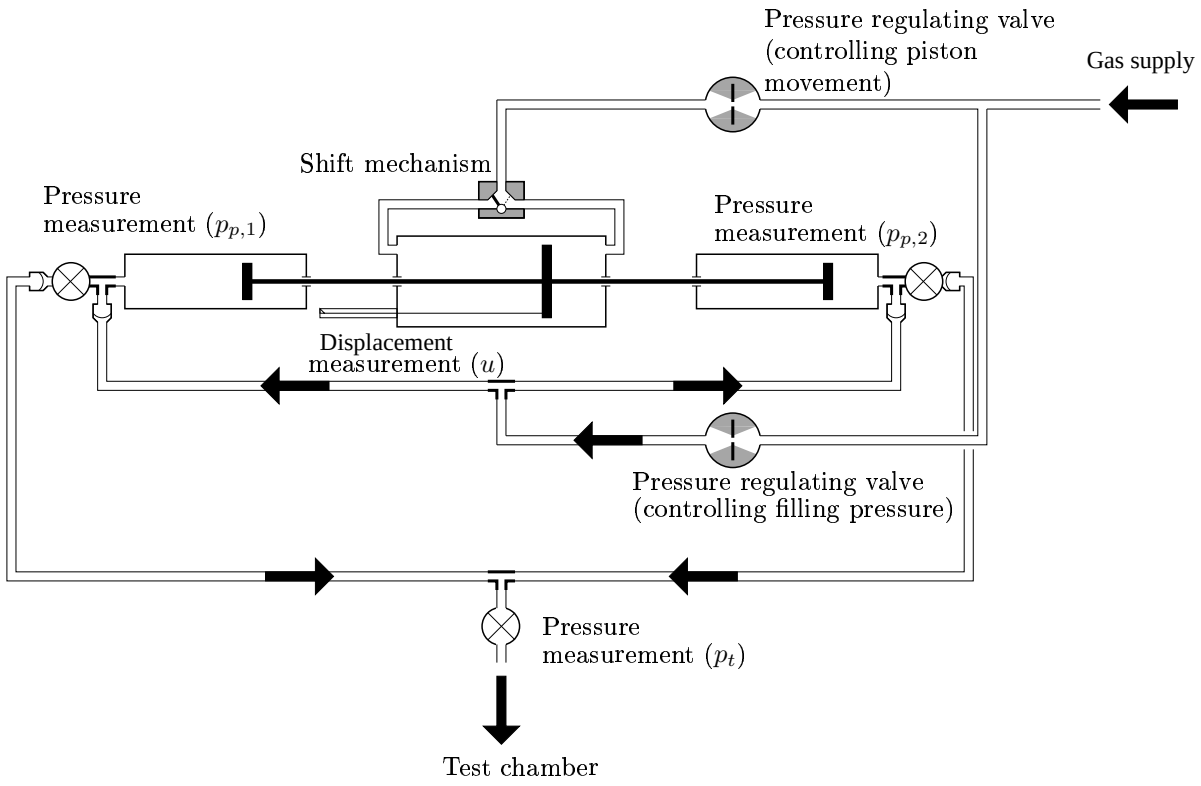

Figure 3.2: Schematic plot of experimental setup used for CPEs

3.2 Determination of k_{int} and b

In this subsection, the determination of the parameters k_{int} and b, introduced in Chapter 2 to describe the permeability for compressible fluids, from DPEs and CPEs is described. For this purpose, the molar flux through the specimen, which is given by $p_t\,Q_t$, where Q_t [m^3/s] is the volume flux at the top surface of the specimen, is required. Taking into account the decrease of p_t during DPEs and slight variations of p_t during CPEs with time, $p_t\,Q_t$ is determined for selected time intervals $t_1 \leq t \leq t_2$, giving – for one experiment – several values for the molar flux as $\overline{p}_t\,Q_t$ corresponding to different time intervals $t_1 \leq t \leq t_2$, where $\overline{p}_t = [p_t(t_2) + p_t(t_1)]/2$. In the following, determination of $\overline{p}_t\,Q$ for one selected time interval from DPEs and CPEs is outlined.

3.2.1 Determination of $\overline{p}_t\,Q_t$ from DPE

During DPEs, the pressure in the test-chamber – container system is continuously decreasing in consequence of air flow through the specimen. The amount of moles of air in the test-chamber – container system for the two time instants t_1 and t_2 is given by the respective pressures $p_{t,1}$ and $p_{t,2}$ by the ideal-gas law as

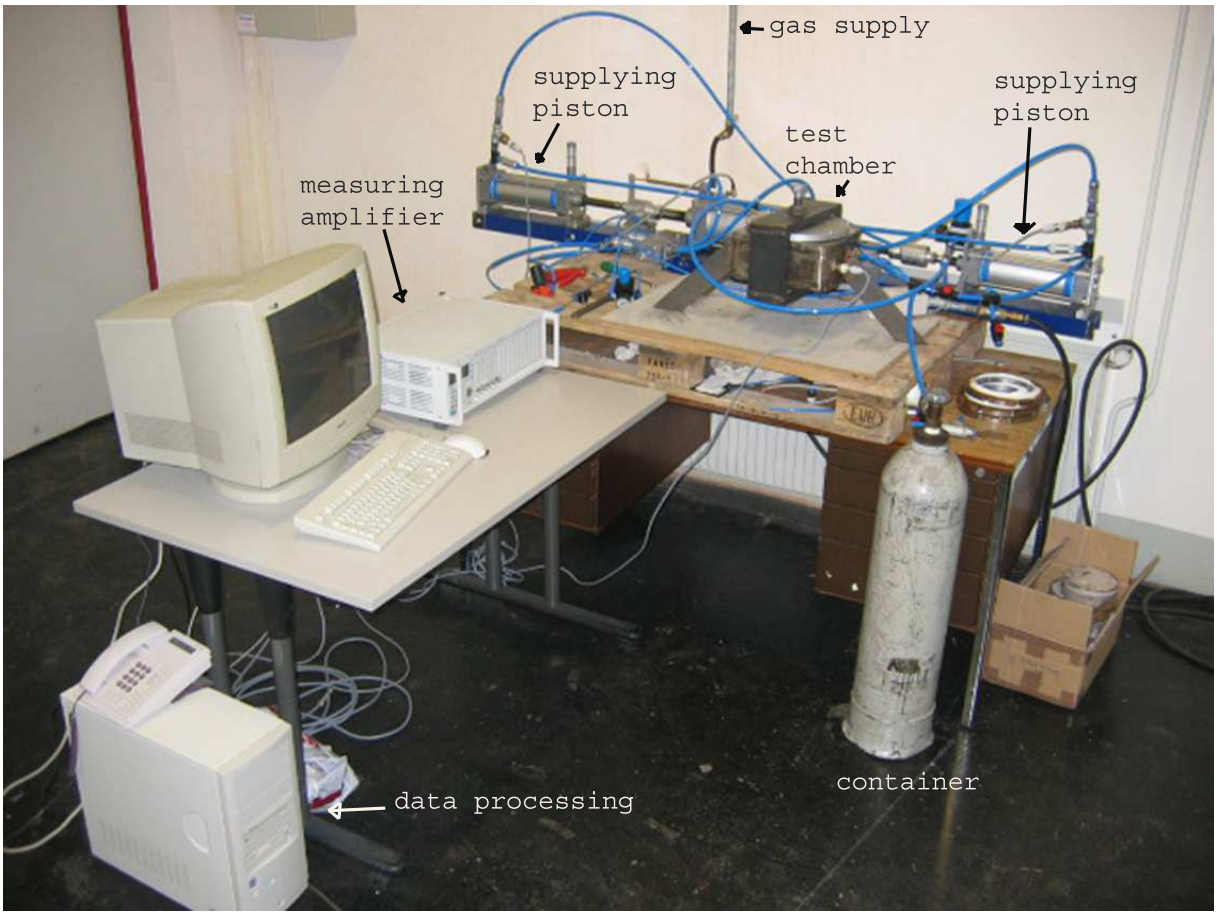

Figure 3.3: Photo of experimental device showing supplying pistons used for CPE and the container used for DPE

$$n_1 = \frac{p_{t,1}\, V_1}{R T_1} \text{ and } n_2 = \frac{p_{t,2}\, V_2}{R T_2}\,, \tag{3.1}$$

where $V_1 = V_2 = V$ [m^3] is the constant volume of the test-chamber – container system, R=8.3144 J/(K mol) is the universal gas constant, and $T_1 = T_2 = T$ [K] is the constant temperature (isothermal conditions). The difference between n_2 and n_1 is the amount of moles that passed through the specimen within $t_1 \leq t \leq t_2$, given from Equations (3.1) as

$$n_1 - n_2 = \frac{(p_{t,1} - p_{t,2})\, V}{R T}. \tag{3.2}$$

On the other hand, the amount of moles passing through the specimen within the time interval $t_1 \leq t \leq t_2$ may be approximated by the incremental form of the ideal-gas law, reading for the case of a constant pressure p:

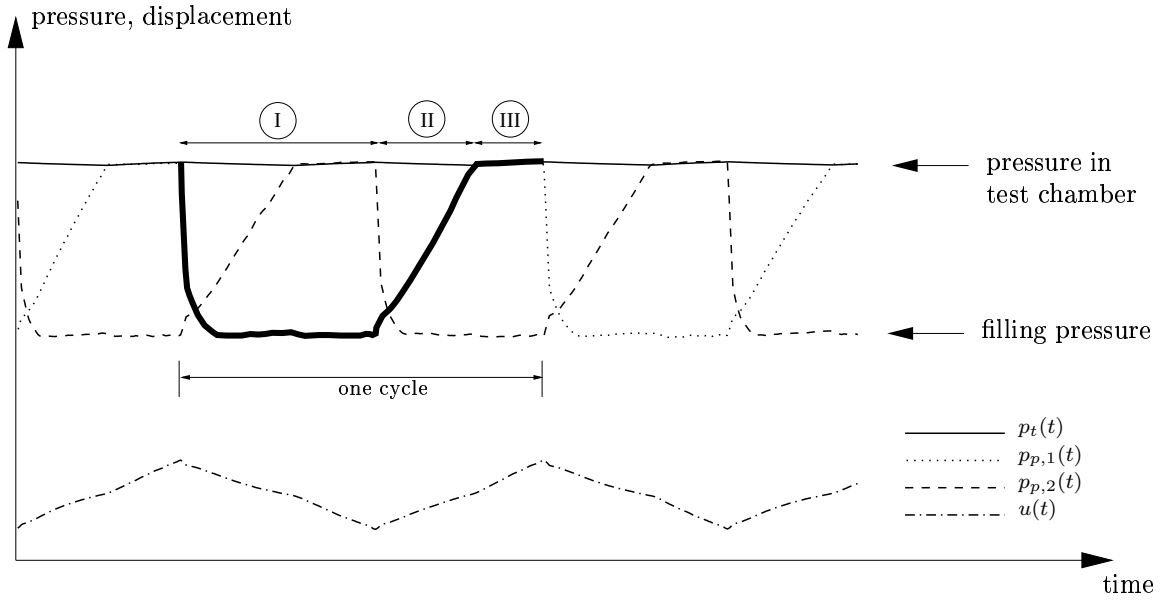

Figure 3.4: Illustration of history of quantities monitored during CPEs: pressure in the test chamber $p_t(t)$ and pressure in the pistons $p_p(t)$; displacement $u(t)$ (filling pressure < test-chamber pressure)

$$\frac{\Delta n}{\Delta t} = p\,\frac{\Delta V}{\Delta t}\,\frac{1}{RT}. \tag{3.3}$$

Rewriting Equation (3.3) for the time interval $t_1 \leq t \leq t_2$ and replacing $p = constant$ by $\overline{p}_t$ and $\Delta V/\Delta t$ by Q_t, one gets

$$\frac{n_1 - n_2}{t_2 - t_1} \approx \overline{p}_t\, Q_t\, \frac{1}{RT}. \tag{3.4}$$

Obviously, the quality of approximation (3.4) depends on the difference between $p_{t,1}$ and $p_{t,2}$ and improves for $p_{t,1}$ getting closer $p_{t,2}$, i.e., for small time intervals $t_1 \leq t \leq t_2$. Combining Equations (3.2) and (3.4), an estimate for the molar flux through the specimen is obtained as

$$\overline{p}_t\, Q_t = \frac{(n_1 - n_2)\, RT}{t_2 - t_1} = \frac{(p_{t,1} - p_{t,2})\, V}{t_2 - t_1}. \tag{3.5}$$

3.2.2 Determination of $\overline{p}_t\, Q_t$ from CPE

During CPEs, two pistons supply air to the test chamber in an alternate manner. Thus, when the air supply shifts from one piston to the other, no air is supplied until the pressure

in the supplying piston is increased from the filling pressure to the pressure in the test chamber as a result of air compression and the respective one-way valves opens. Since no air is supplied during this time, the pressure in the test chamber slightly decreases.
Each cycle of one of the two pistons is divided into three phases (see Figure 3.4):

- Filling phase (I): The piston is filled with air giving a pressure equal to the pressure of the gas supply (filling pressure). The piston is in its backward movement. The one-way valve to the test chamber is closed (piston pressure < test-chamber pressure).
- Air-compression phase (II): The pressure in the piston increases gradually during movement. The one-way valve to the test chamber (piston pressure < test-chamber pressure) and the one-way valve to the air supply (filling pressure < piston pressure) are closed.
- Air-supply phase (III): The pressure in the piston exceeds the pressure in the test chamber. The one way valve to the test chamber opens and air is supplied to the test chamber.

In the following, two modes of determining $\overline{p}_t\, Q_t$ from CPEs are presented.

Mode I - considering Phase III of piston movement only

The history of the test-chamber pressure p_t(t) during Phase III of the piston movement is accessible via the installed pressure gauge (see Figure 3.4). During Phase III, this pressure is slightly increasing. Applying the ideal-gas law for two selected time instants within Phase III, t_1 and t_2, the moles of air are obtained as

$$n_1 = \frac{p_{t,1}\, V_1}{RT} \text{ and } n_2 = \frac{p_{t,2}\, V_2}{RT}\,, \tag{3.6}$$

where V_1 [m^3] and V_2 [m^3] are given by

$$V(t) = V_{Chamber} + V_{Container} + V_{Pipe} + V_{Piston}\,\frac{1-u(t)}{L}, \tag{3.7}$$

with $V_{Chamber}$,$V_{Container}$,V_{Pipe}, and V_{Piston} representing the volume of the test chamber, the container, the connecting pipes, and the piston, respectively (see Table 3.1). In Equation (3.7), L =132.7 mm is the total heave of the piston and $u(t)$, with $0 \leq u(t) \leq L$, is the actual displacement monitored during CPEs. The volume flux through the specimen is calculated by inserting Equation (3.6) into Equation (3.4), giving

$$\overline{p}_t\, Q_t = \frac{p_{t,1}\, V_1 - p_{t,2}\, V_2}{t_2 - t_1}. \tag{3.8}$$

Test chamber	4.942 liter
Container	20.8 liter
Connecting pipes	0.295 liter
Piston	0.116 liter

Table 3.1: Volume of different parts of the CPE setup

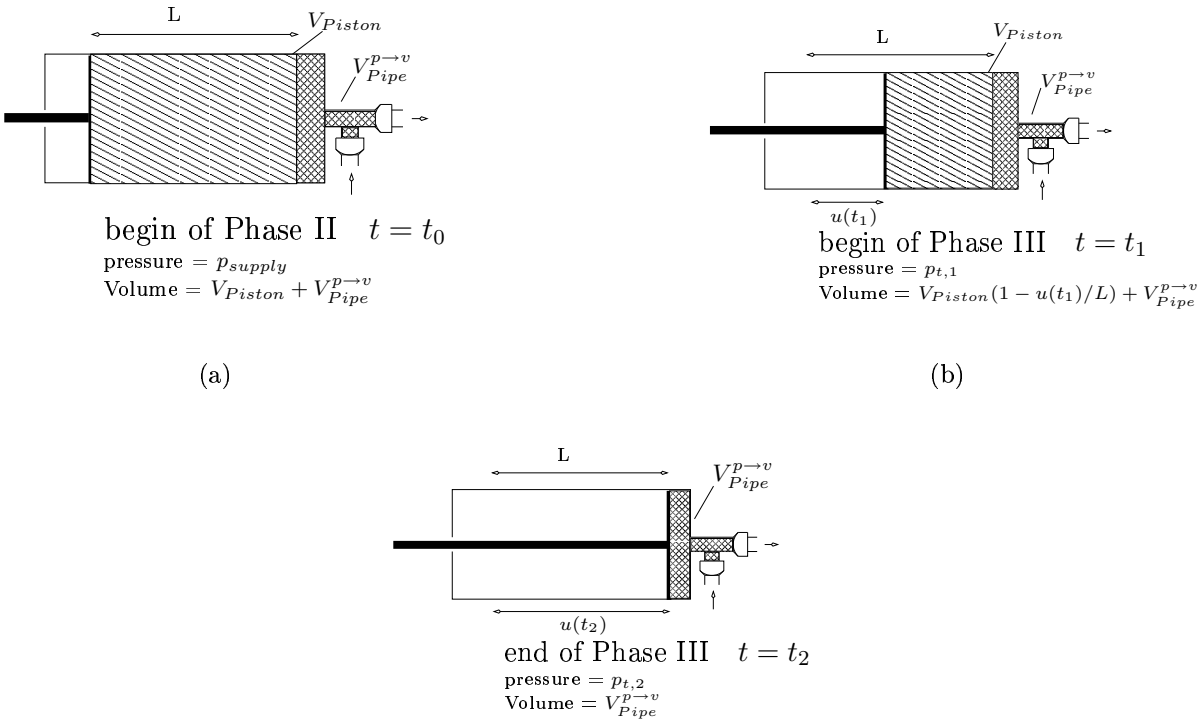

Figure 3.5: Positions of piston during one cycle ($V_{Pipe}^{p\to v}$ represents the part of the pipe volume from the piston to the two one-way valves only)

Mode II - considering the piston cycle

For this mode of determining $\overline{p}_t\, Q_t$, the moles of air provided to the test chamber during each piston movement cycle are considered. For this purpose, the amount of moles within the piston and the pipes connecting the piston with the two one-way valves is determined

from

$$\text{Figure 3.5 (a): } n_0 = \frac{p_{t,0}\,(V_{Piston} + V_{Pipe}^{p\to v})}{RT}, \tag{3.9}$$

$$\text{Figure 3.5 (b): } n_1 = n_0 = \frac{p_{t,1}\left[V_{Piston}\left(1 - \frac{u(t_1)}{L}\right) + V_{Pipe}^{p\to v}\right]}{RT}, \tag{3.10}$$

$$\text{Figure 3.5 (c): } n_2 = \frac{p_{t,2}\,V_{Pipe}^{p\to v}}{RT}, \tag{3.11}$$

where $n_0 = n(t_0)$, $n_1 = n(t_1)$, and $n_2 = n(t_2)$. Combining Equations (3.9) and (3.10) gives access to the pipe volume from the piston to the one-way valves, $V_{Pipe}^{p\to v}$, with

$$V_{Pipe}^{p\to v} = \frac{p_{t,0}\,V_{Piston} - p_{t,1}\left(1 - \frac{u(t_1)}{L}\right)}{p_{t,1} - p_{t,0}}. \tag{3.12}$$

Finally, the amount of moles provided to the test chamber during one cycle of the pressure piston is given by $n_1 - n_2$, reading

$$n_1 - n_2 = \frac{1}{RT}\left[p_{t,1}\,V_{Piston}\left(1 - \frac{u(t_1)}{L}\right) + V_{Pipe}^{p\to v}\,(p_{t,1} - p_{t,2})\right]. \tag{3.13}$$

With Equation (3.13) at hand and considering that the second piston supplies air when the considered piston is in its backward movement, $\overline{p}_t\,Q_t$ is determined from Equation (3.4), which becomes for the forward movement of the considered piston

$$\overline{p}_t\,Q_t = \frac{(n_1 - n_2)\,RT}{t_2 - t_0}, \tag{3.14}$$

where $t_2 - t_0$ is the time span in which the considered pressure piston is in its forward movement (Phase II and Phase III).

3.2.3 Determination of k_{int} and b from $\overline{p}_t\,Q_t$

Based on the given values for $\overline{p}_t\,Q_t$, the parameters k_{int} and b are determined. For this purpose, Equation (2.2) is inserted into Equation (2.1) and multiplied by p, giving a differential equation for the pressure over the specimen height

$$p(x)\,Q(x) = \frac{k_{int}\,A}{\eta}\frac{d\,p}{d\,x}\,[p(x)+b], \tag{3.15}$$

where $q = Q/A$, with A as the cross-section of the cylindrical specimens, was considered. Rewriting Equation (3.15) for the mean pressure $\overline{p}_t$ between two time instants t_1 and t_2 and taking into account that $\overline{p}\,Q$, which is known at the top surface of the specimen (see determination of $\overline{p}_t\,Q_t$ in previous subsections), is constant over the specimen height, the pressure p_b at the bottom surface of the specimen is obtained from the repeated approximation of the pressure distribution, following (see Figure 3.6)

$$p(x_{i+1}) = p(x_i) + \frac{d\,p}{d\,x}\Big|_{x_i}\frac{h}{n} = p(x_i) - \frac{\overline{p}_t\,Q_t\,\eta}{[p(x_i)+b]\,A\,k_{int}}\,\frac{h}{n}, \tag{3.16}$$

where h is the specimen height, n represents the number of intervals considered over the specimen height, and $p(x_1) = p_1 = \overline{p}_t$.

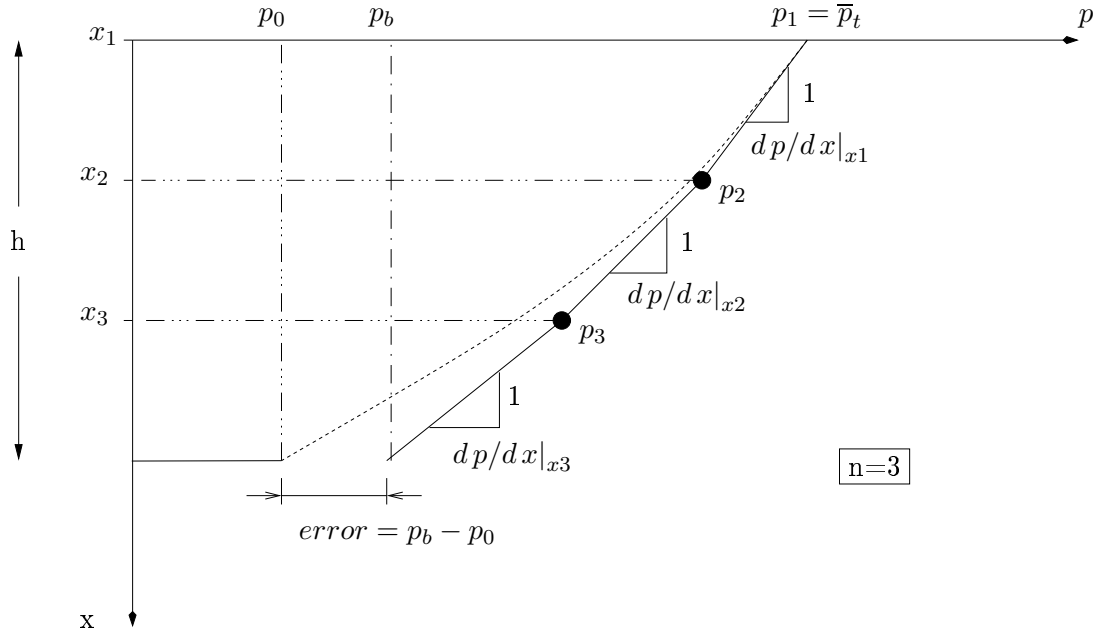

Figure 3.6: Determination of p_b by repeated application of Equation (3.16)

The pair of k_{int} and b minimizing the error R, with

$$R(k_{int}, b) = \frac{1}{n_t}\sqrt{\sum_{j=1}^{n_t}\{\,p_b\,[(\overline{p}_t\,Q_t, \overline{p}_t)^j; k_{int}, b] - p_0\}^2} \tag{3.17}$$

where n_t represents the number of time intervals $t_1 \leq t \leq t_2$ specified for each experiment, is determined by a search algorithm. Hereby, the initial search interval is set according to previous studies as $0.1 \leq k_{int} \leq 10000$ nm^2 and $0.1 \leq b \leq 500$ bar.

Alternatively, k_{int} and b are determined using the procedure outlined in (Leithner 2004). Hereby, based on a linear pressure distribution over the specimen height, the apparent permeability k is determined for the time interval $t_1 \leq t \leq t_2$ as

$$k = \frac{\overline{p}_t \, Q_t \, h \, \eta}{A \, (\overline{p}_t^2 - p_0^2)}, \tag{3.18}$$

where $\overline{p}_t \, Q_t$ is obtained from Subsections 3.2.1 and 3.2.2. Based on the values for k computed for different time intervals and pressure levels $\overline{p}_t = [p_t(t_1) + p_t(t_2)]/2$, k_{int} and b are obtained from linear approximation of k in the $k - 1/\overline{p}$ diagram (see Figure 2.1). Hereby, k_{int} is given by extrapolation of this linear approximation function towards $1/\overline{p} = 0$, i.e., towards the theoretical case of infinite pressure.

The number n_t and the size of the time intervals, $\Delta t = t_2 - t_1$, for each type of experiment are specified as:

- In the course of DPEs, the pressure in the test-chamber – container system decreases gradually. Depending on the duration of the DPE, which itself depends on the permeability and, thus, on the pre-heating temperature, the size of the interval was chosen either 100 or 1000 seconds. The number of time intervals, n_t, is obtained from the duration of the experiment, i.e., the time span for the pressure to decrease from 8 to 2 bar, divided by either 100 or 1000.

- Accounting for sudden pressure changes in consequence of piston movement during CPEs, a time interval of $0.1 \leq \Delta t \leq 4$ seconds was considered during determination of k_{int} and b. Accordingly, the number of time intervals, n_t, depends on the duration of the experiment (usually 20 minutes), the rate of the piston movement (depending on the permeability), and the analysis mode employed (see Subsection 3.2.2).

Chapter 4

Materials

In this thesis, the transport properties of a concrete similar to the lining concrete used at the Lainzer Tunnel (Kusterle et al. 2004) was investigated. The mix design of this concrete is given in Table 4.1.

	Lainz	Block 1	Block 2
Cement (PZ 375 HS C3A frei) [kg/m^3]	260	260	260
Fly ash (Flural - Draurecycling) [kg/m^3]	260	60	60
Liquifier (Readyplast P1) [kg/m^3]	3.1	3.1	3.1
Superplasticiser (Readyplast SP - NA) [kg/m^3]	3.5	3.5	3.5
Airtrainer (Readyair A1) [kg/m^3]	0.9	0.9	0.9
Water content [kg/m^3]	157	120	129
Polypropylene Fibers [kg/m^3]		0.0	1.5
Aggregates [kg/m^3]	1909	1942	1942
Aggregate fraction 0 - 4 mm [mass- %]	45	46	46
Aggregate fraction 4 - 16 mm [mass- %]	36	35	35
Aggregate fraction 16 - 324 mm [mass- %]	19	19	19
Water content[1] [kg/m^3]	157	157	167
Water/cement-ratio [-]	0.60	0.60	0.60
Water/binder-ratio [-]	0.49	0.49	0.54

[1] 2 mass-% of the aggregate for Block 1 and 2 included (wet aggregate)

Table 4.1: Mix design of concrete considered in this thesis (two blocks of concrete were produced)

Two blocks (length × width × height = 0.75 × 0.3 × 0.3 m) were produced (see Figure

4.1). One block was made of concrete with no fibers, whereas 1.5 kg/m^3 PP-fibers (diameter of approximately 22 μm and a length of 6 mm) were added to the concrete of the second block. As the fibers reduced the workability, 9 kg water were added in order to provide proper densification of the fresh concrete (see Table 4.1).
After concreting, the blocks were stored at room temperature for 28 days. Then, cores with a diameter of 150 mm were obtained from drilling. These cores were cut into pieces of 50 mm height, giving the test specimens (see Figure 4.1).
The specimens were stored at 80 °C in order to ensure equal saturation for all specimens. Before the permeability test, the specimens were heated by a heating rate of 1 °C/min to their respective target temperature. At this temperature, the specimens were stored from 20 to 60 hours (depending on the target temperature). Thereafter, the temperature was decreased by a cooling rate of 1 °C/min.
The final preparation of the specimen for the permeability test included filling of holes at the top and bottom of the specimen with a size exceeding 5 mm in depth, sealing of the side surface of the specimen, and connecting the specimen to the support ring with silicone. Figure 4.2 shows a specimen right before testing.

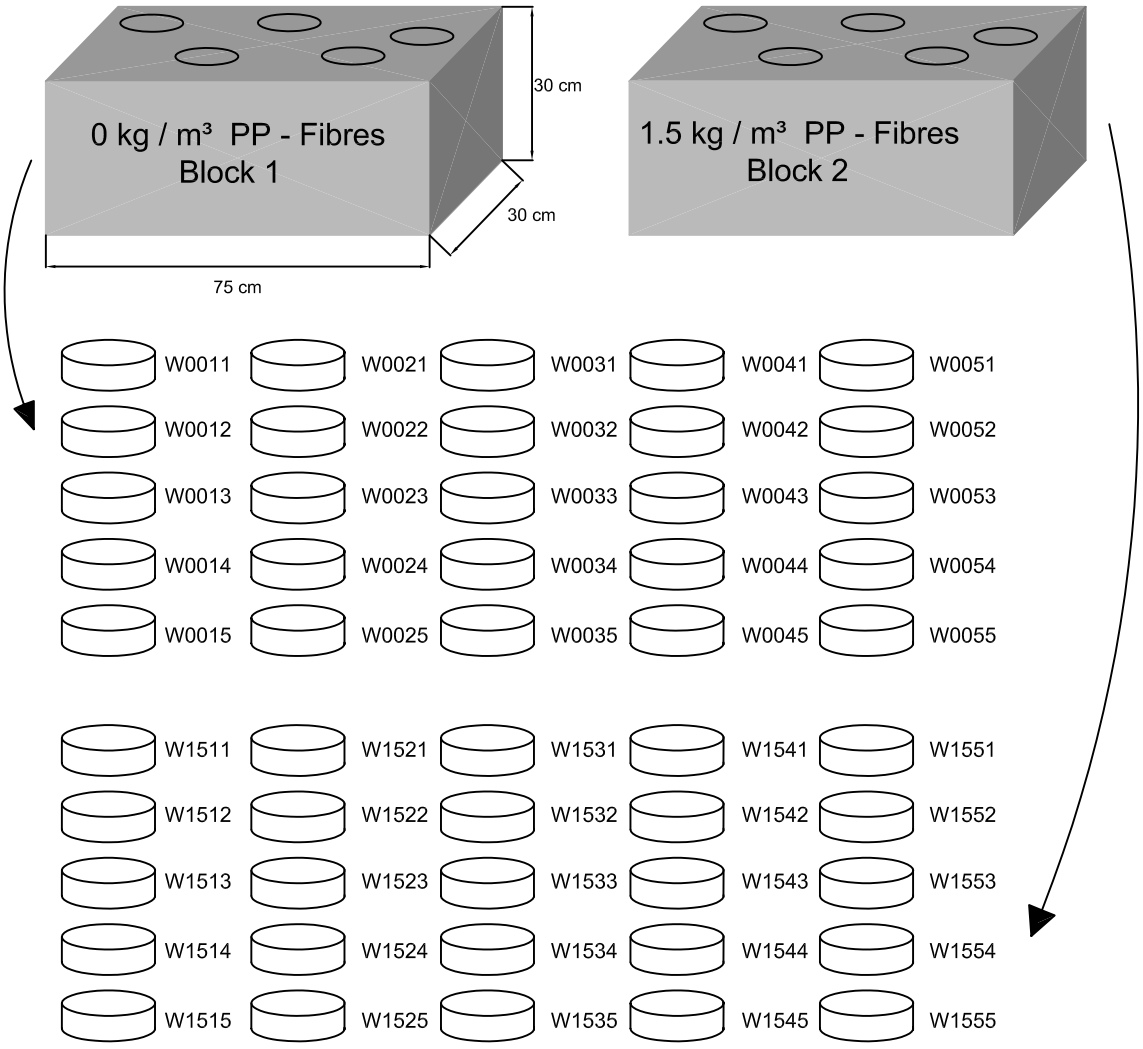

Figure 4.1: Location of specimen within the produced concrete blocks

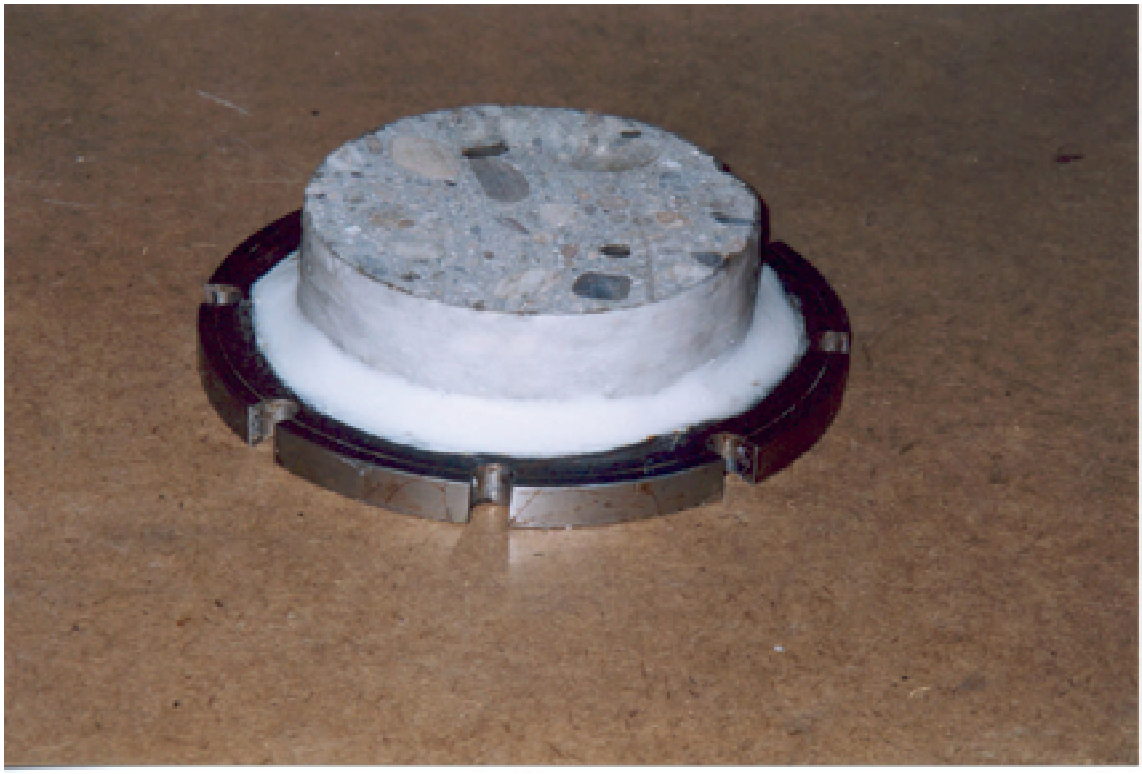

Figure 4.2: Specimen connected to support ring prepared for permeability testing

Chapter 5

Presentation of results

Table 5.1 gives an overview about the experiments performed in the course of this thesis. Hereby, "d" and "c" stand for DPE and CPE, respectively. In addition to the experiments listed in Table 5.1, data reported in (Leithner 2004) was included in the presentation of results (see Table 5.2).

Figures 5.1 to 5.6 show the intrinsic permeability k_{int} and the parameter b for specimens with and without PP-fibers. For both types of concrete, a clear trend of increasing intrinsic permeability with temperature can be observed. The large scatter of test results for a pre-heating temperature lower than 80°C (see, e.g., Figure 5.5) is explained by the presence of capillary water. With increasing temperature, the capillary water is removed and the obtained results show less scatter. Concrete specimens with no PP-fibers exhibit a steady (almost linear) increase of the permeability with temperature. Experiments conducted in the course of this thesis and the ones of Leithner (2004) show this trend. For concrete specimens with PP-fibers, a strong increase of the permeability between 80°C and 170°C can be observed. This increase, however, seems to be more pronounced for experiments conducted in the course of this thesis.

The obtained values for the parameter b does not show a clear trend with increasing temperature. At all pre-heating temperatures, the values of b show a significant scatter.

specimen	80°C	105°C	169°C	224°C	329°C	423°C
w0012	c/d	c			c/d	
w0013	c/d			c		
w0022	c		c/d			
w0024	c/d	c/d			c/d	
w0032	c					c/d
w0033	c			c/d		
w0042	c		c			
w0043	c/d					c/d
w0044	c	c			c	
w0052	c			c		
w0054	c		c/d			
w1512	c	c/d			c	
w1514	c		c			
w1522	c			c		
w1523	c/d					c/d
w1524	c	c/d			c/d	
w1532	c			c/d		
w1533	c					c
w1543	c		c			
w1544	c/d			c		
w1552	c		c/d			
w1553	c	c			c/d	
w1554	c/d					c

Table 5.1: Conducted permeability test ("c" and "d" stand for CPE and DPE, respectively)

specimen	20°C	80°C	105°C	140°C	200°C	300°C	400°C	600°C
of1/1	d			d				
of1/2	d				d			
of1/3		d					d	
of2/1	d					d		
of2/2	d		d					
of2/3		d						
of3/1	d							d
of3/2	d						d	
of3/3						d		
of4/1	d			d				
of4/2	d		d					
of4/3				d				
of5/1	d	d						
of5/2	d					d		
of5/3								d
mf1/1	d							
mf1/2	d			d				
mf1/3		d					d	
mf2/1	d					d		
mf2/2	d		d					
mf2/3		d						d
mf3/1	d							d
mf3/2	d						d	
mf3/3		d	d					
mf3/4		d		d				
mf4/1		d			d			
mf4/2		d				d		
mf4/3				d				

Table 5.2: Permeability tests conducted in (Leithner 2004) ("d" stands for DPE)

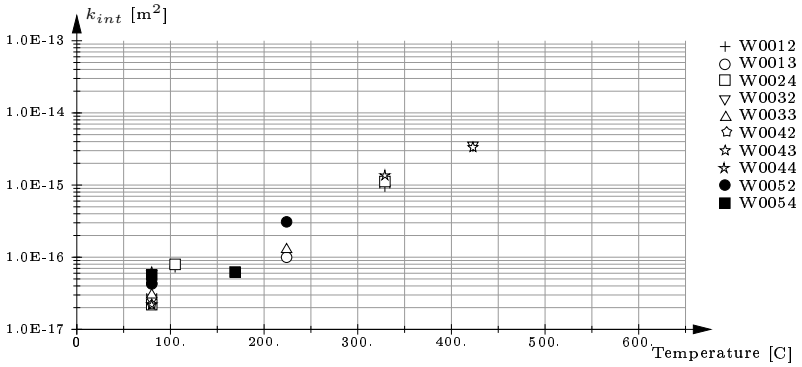

(a) CPE - mode I

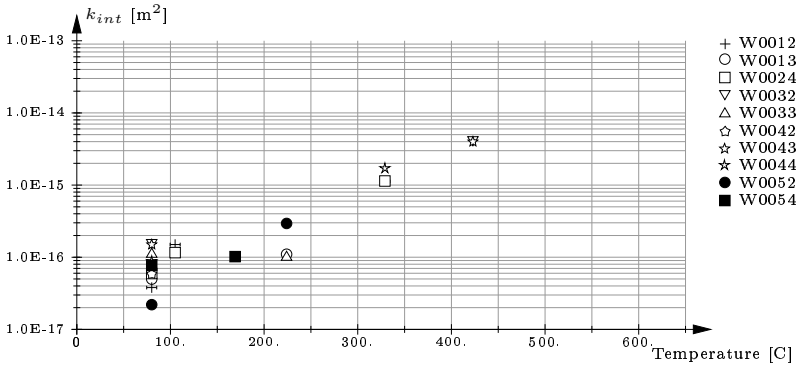

(b) CPE - mode II

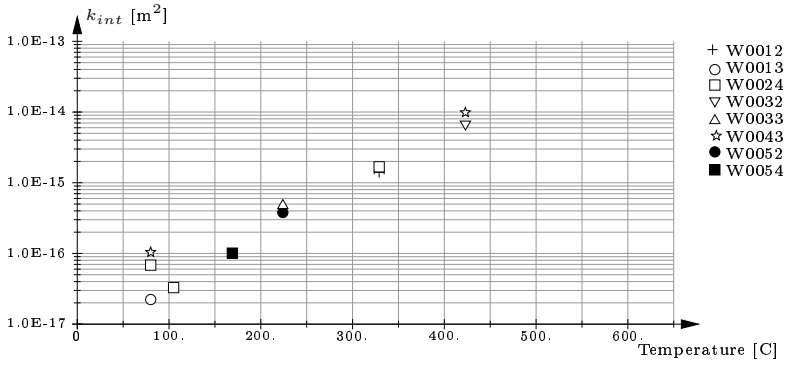

(c) DPE

Figure 5.1: Intrinsic permeability k_{int} for concrete with no PP-fibers (test results from this thesis)

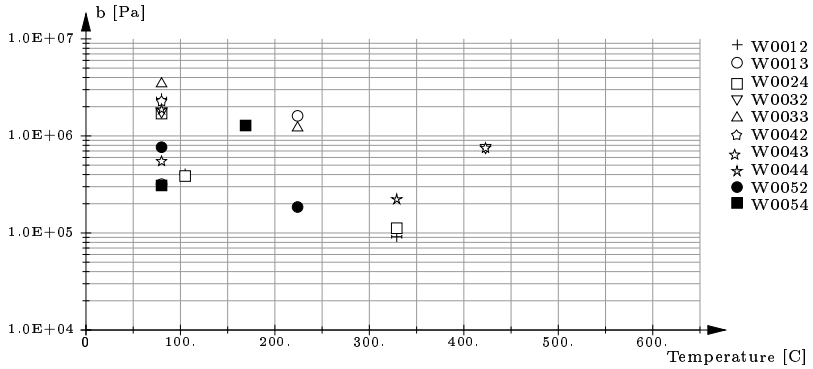

(a) CPE - mode I

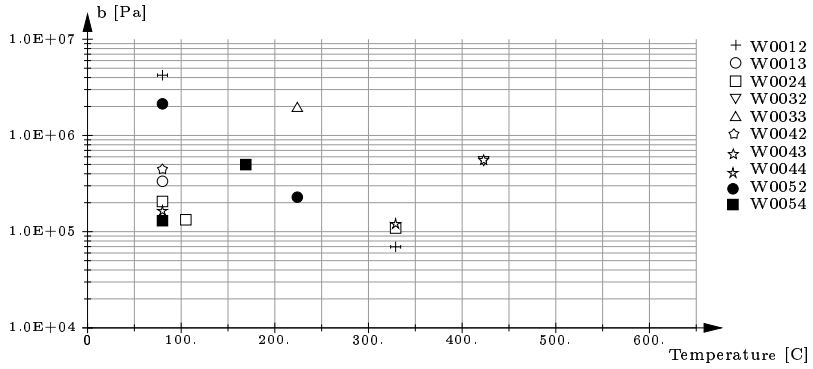

(b) CPE - mode II

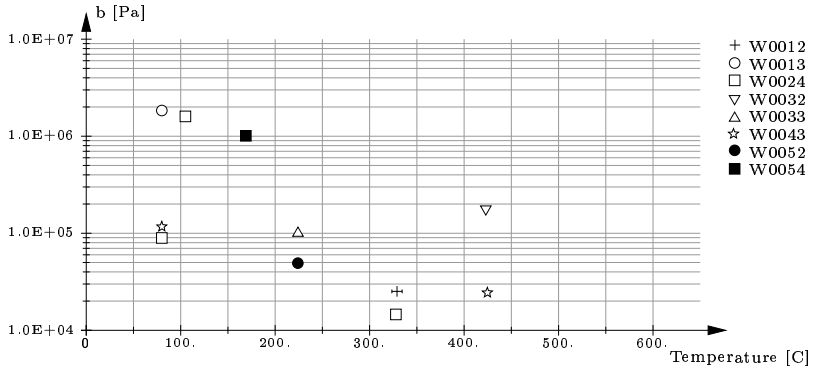

(c) DPE

Figure 5.2: Parameter b for concrete with no PP-fibers (test results from this thesis)

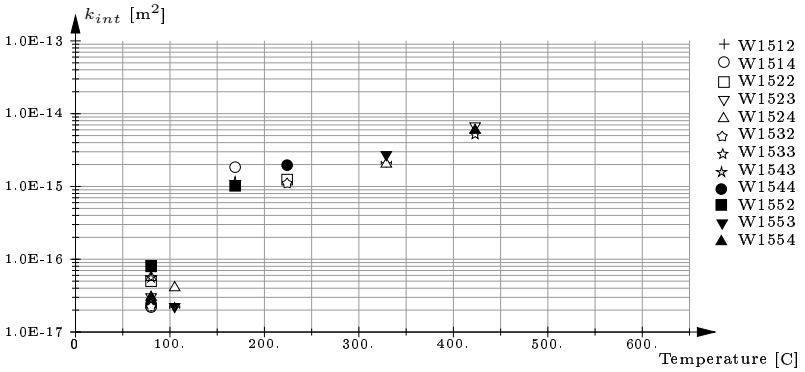

(a) CPE - mode I

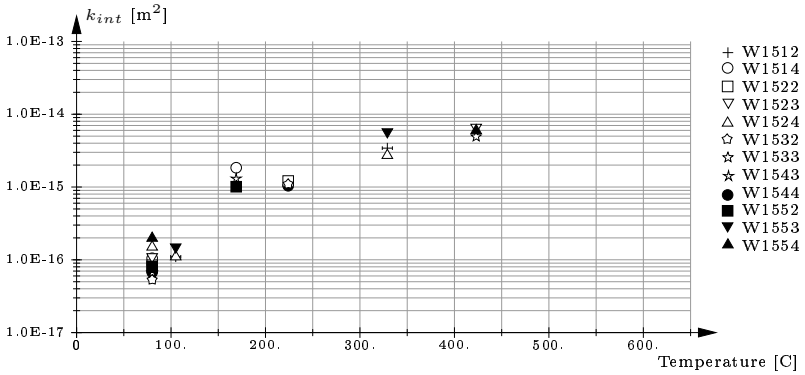

(b) CPE - mode II

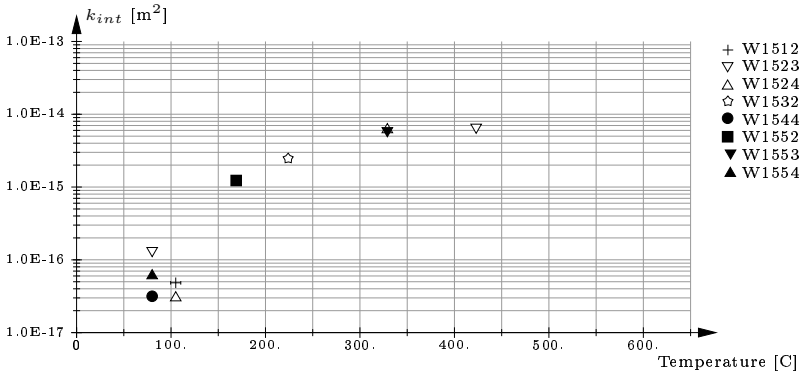

(c) DPE

Figure 5.3: Intrinsic permeability k_{int} for concrete with PP-fibers (test results from this thesis)

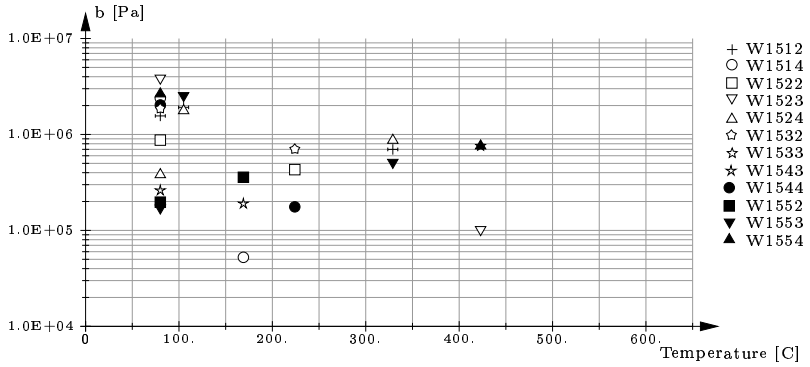

(a) CPE - mode I

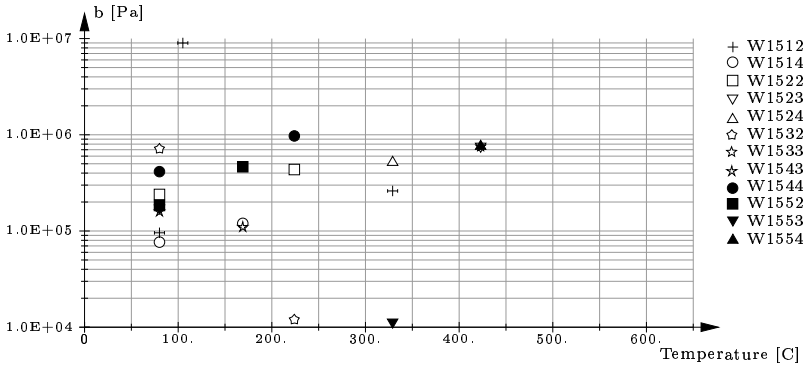

(b) CPE - mode II

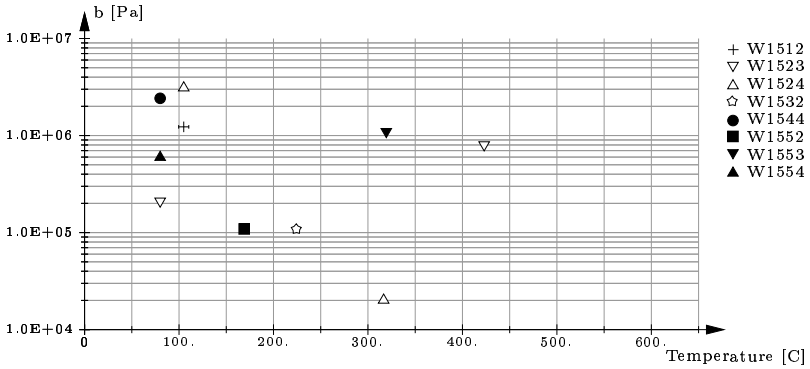

(c) DPE

Figure 5.4: Parameter b for concrete with PP-fibers (test results from this thesis)

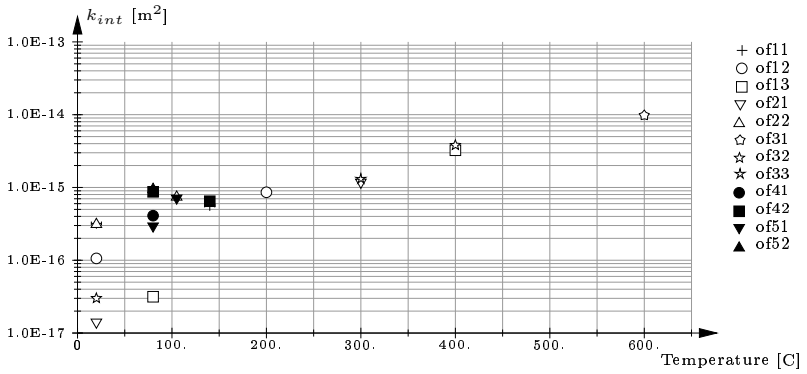

(a) DPE

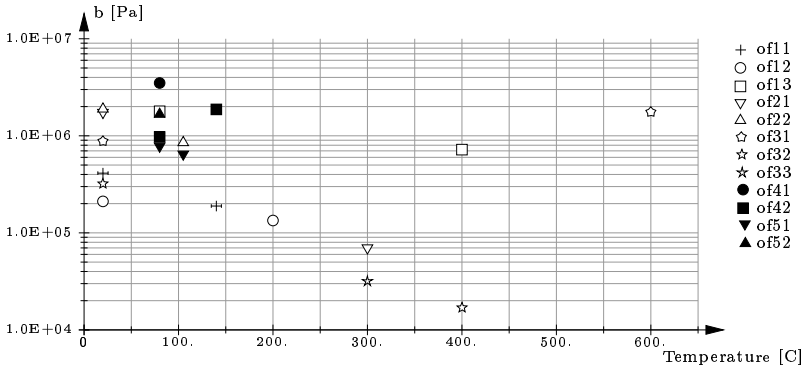

(b) DPE

Figure 5.5: Intrinsic permeability k_{int} and parameter b for concrete with no PP-fibers (test results from (Leithner 2004))

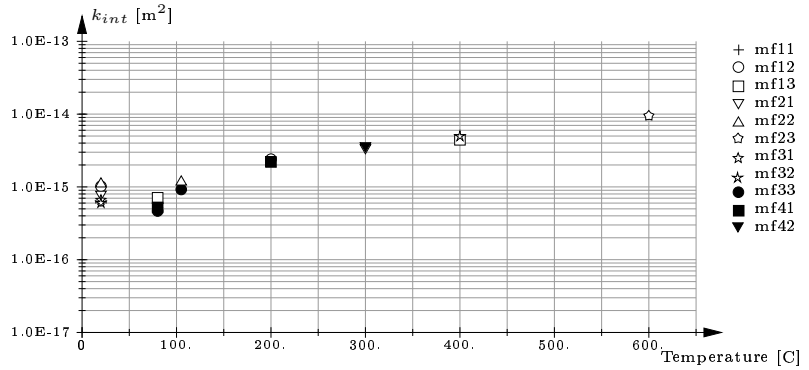

(a) DPE

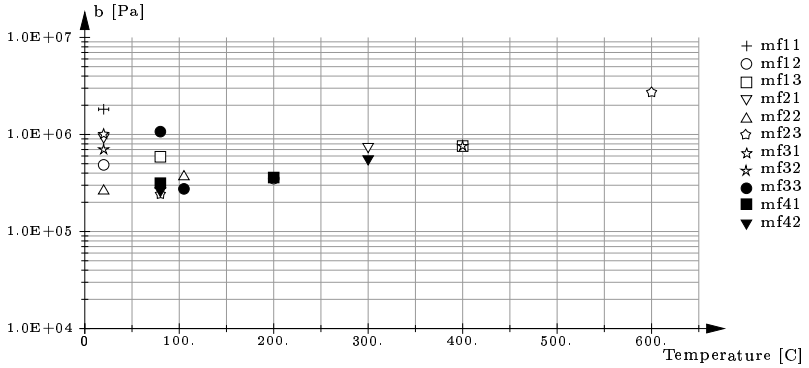

(b) DPE

Figure 5.6: Intrinsic permeability k_{int} and parameter b for concrete with PP-fibers (test results from (Leithner 2004))

Chapter 6

Discussion

6.1 Stress analysis

In the course of the permeability experiments, specimens are loaded by gas pressures up to 9 bar (9×10^5 Pa), which might initiate tensile failure at the bottom surface of the specimens and, thus, increase the permeability.

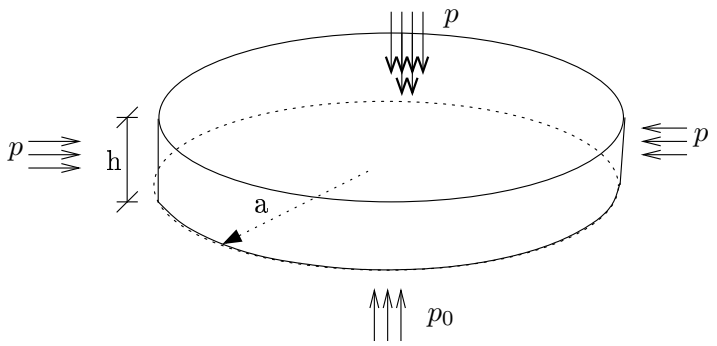

Figure 6.1: Schematic plot of specimen under pressure

According to Mehlhorn (1996), the maximal moment for a circular plate under pressure applied onto the top surface becomes

$$M_{max} = -2\,(1+\nu)\,K\,B, \tag{6.1}$$

where ν is the Poisson's ratio, and K and B are given for the case of a sliding support by

$$K = \frac{E\,h^3}{12(1-\nu^2)} \text{ and } B = -\frac{3+\nu}{1+\nu}\,\frac{(p-p_0)\,a^2}{32\,K} \quad . \tag{6.2}$$

The tensile stress at the bottom surface of the specimen is equal to the sum of $M_{max}/(h^2/6)$ and the stress resulting from the pressure at the side surface, giving

$$\sigma_{max} = 2\,(1+\nu)\frac{3+\nu}{1+\nu}\,\frac{(p-p_0)\,a^2}{32}\,\frac{6}{h^2} - p = \left(\frac{3\,a^2\,(3+\nu)}{8\,h^2} - 1\right)\,p\, - \frac{3\,a^2\,(3+\nu)\,p_0}{8\,h^2}. \tag{6.3}$$

Considering ν=0.15, h=50 mm, and a=75 mm, Equation (6.3) gives σ_{max}=1.66 p − 2.66 p_0 [MPa]. Taking into account the temperature dependence of the tensile strength of concrete (see Figure 6.2(a)), σ_{max}=1.66 p−2.66 $p_0 \leq f_t(T)$ must hold (see Figure 6.2(b)). According to Figure 6.2(b), the tensile strength corresponding to a pre-heating temperature of 423°C is higher than the tensile stress resulting from an applied pressure of 9 bar. Thus, cracking did not occur and the mechanical load did not – according to Figure 6.2(b) – influence the permeability measurements. Moreover, the situation depicted in Figure 6.2(b) represents the worst case. Taking into account the confining action of the support ring (departing from the assumption of a sliding support) would result in a reduction of σ_{max}.

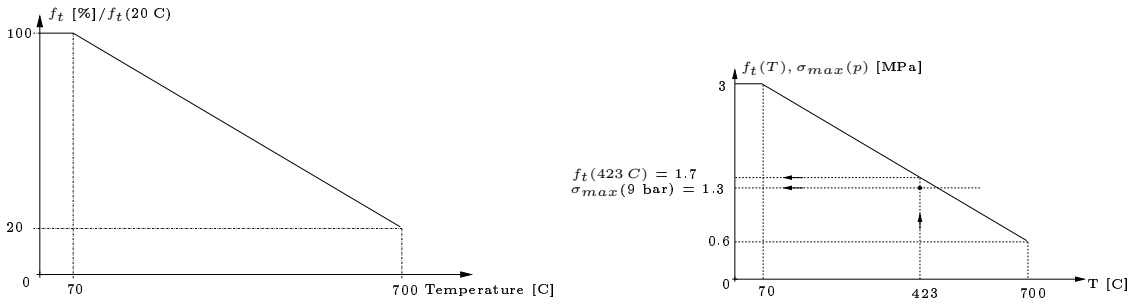

(a) (b)

Figure 6.2: (a) Temperature dependence of tensile strength of concrete according to (EC2 1992) and (b) admissible pressure as a function of temperature for f_t(20°C)= 3 MPa

6.2 Sensibility analysis

The intrinsic permeability k_{int} and the parameter b were determined according to the analysis scheme outlined in Subsection 3.2.3. Hereby, the error function $R(k_{int}, b)$ was

minimized with the absolute minimum providing the final values for k_{int} and b. In order to study the characteristics of this error function (existance of local minima and sensibility with respect to k_{int} and b), the distribution of the error function R for four subsequent search areas is given in Figure 6.3. The dots in Figure 6.3 indicate that the pressure p became negative during repeated application of Equation (3.16) for the considered values of k_{int} and b. The circle indicates the (k_{int},b)-pair giving the minimum value of the error function for the respective search interval. Proper values for k_{int} and b are obtained when the location of the minimum of the error function is not found at the boundary to the area where the values for k_{int} and b resulted in a negative pressure in the specimen (dotted area in Figure 6.3).

The distribution of the error function R given in Figure 6.3 was obtained from CPE-mode II applied to the CPE results for the Specimen W0024. Figure 6.4 shows the error distribution within $1211 \leq k_{int} \leq 1243$ nm^2 and $0.62 \leq b \leq 0.78$ bar, providing insight into the sensibility of the error function with respect to changes of k_{int} and b, giving

$$\frac{\Delta k_{int}}{k_{int}} = \frac{3}{1227} = 0.0024, \tag{6.4}$$

$$\frac{\Delta b}{b} = \frac{0.01}{0.7} = 0.0143, \tag{6.5}$$

where Δk_{int} and Δb (Figure 6.4) were scaled to the values of k_{int} and b corresponding to the minimum of the error function. Equations (6.4) and (6.5) show that an increase of k_{int} by 2.4 ‰ has the same impact on the value of the error function as an increase of b by 14.3 ‰. Accordingly, the value of k_{int} has a higher impact on the error function and, thus, is expected to have a higher accuracy than the value of b.

6.3 Comparison of analysis methods

In contrast to the mode of determination of k_{int} and b presented in this thesis, application of Equation (3.18) (Leithner 2004) assumes a linear pressure distribution over the specimen height (see Figure 6.5). Figure 6.6 shows a comparison of values for k_{int} and b obtained from both modes of analysis. According to Figure 6.6, application of Equation (3.18) generally result in an overestimation of the intrinsic permeability k_{int}. As regards the values of the parameter b, no trend is observed.

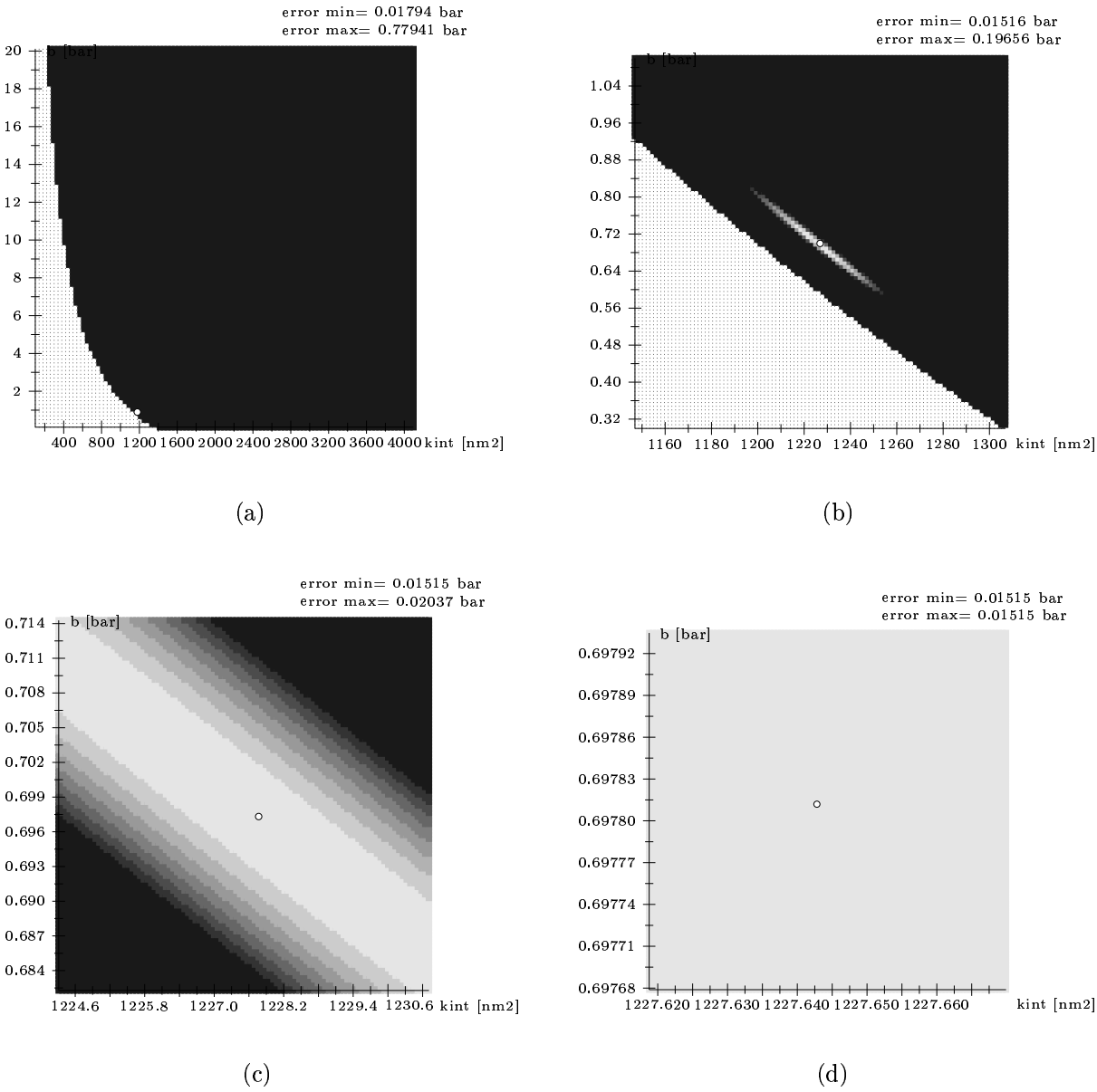

Figure 6.3: Distribution of error function R for four subsequent search areas during determination of k_{int} and b from CPE results of Specimen W0024 employing the analysis mode CPE-mode II (light grey: $R_{min} \leq R \leq 1.01\,R_{min}$; black: $R > 1.1\,R_{min}$)

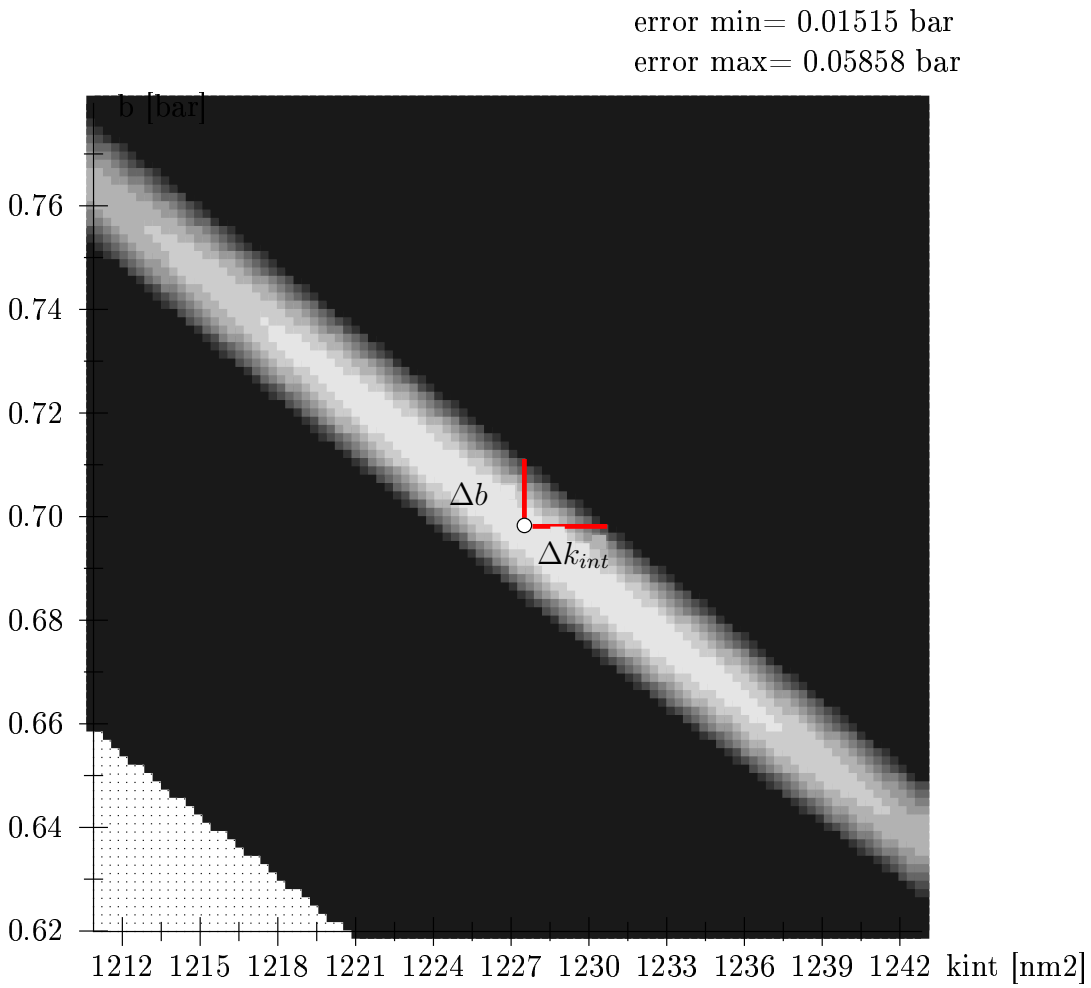

Figure 6.4: Distribution of error function R for $1211 \leq k_{int} \leq 1243$ nm^2 and $0.62 \leq b \leq 0.78$ bar for Specimen W0024 employing the analysis mode CPE-mode II (light grey: $R_{min} \leq R \leq 1.01\, R_{min}$; black: $R > 1.1\, R_{min}$)

6.4 DPE versus CPE

The experimental setup presented in this thesis allows conduction of DPEs and CPEs. Whereas DPEs are easier to conduct and require less time, CPEs are required for specimens characterized by a high permeability in order to provide (in average) stationary conditions.

Figure 6.7 shows a comparison of results obtained from DPEs and CPEs. Both experiments yield similar results. However, DPEs rely on a strong difference between the time scale associated with the pressure decrease in the test-chamber – container system and the time scale associated with air transport through the specimen. Only in case characterized by a pressure decrease significantly slower than the time scale of air transport

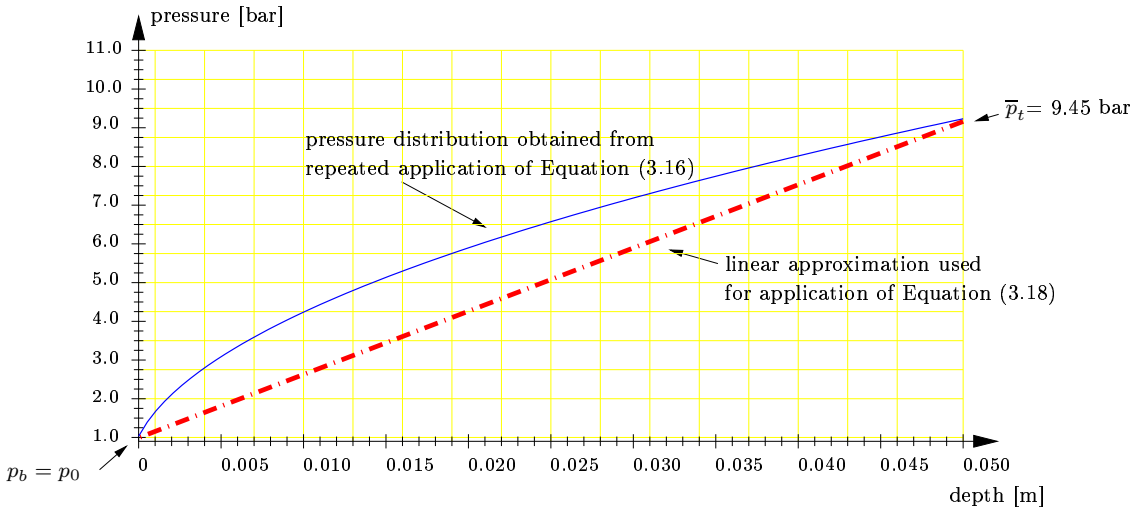

Figure 6.5: Pressure distribution over specimen height for Specimen W1514 ($\overline{p}_t\, Q_t$=5.4E-06 m^3/s bar, $\overline{p}_t$=9.45 bar)

through the specimen, the assumption of stationary conditions during determination of $\overline{p}_t\, Q_t$ is valid. Thus, for specimens exhibiting a high permeability, the pressure decrease occurs faster and the DPE might deliver erroneous results. However, in the present study considering pre-heating temperatures up to 423°C with permeabilities k up to k=$k_{int}\,(1 + b/\overline{p})$=20000(1+500/2)=520000 nm^2 (5.2E-13 m^2) this was not the case.

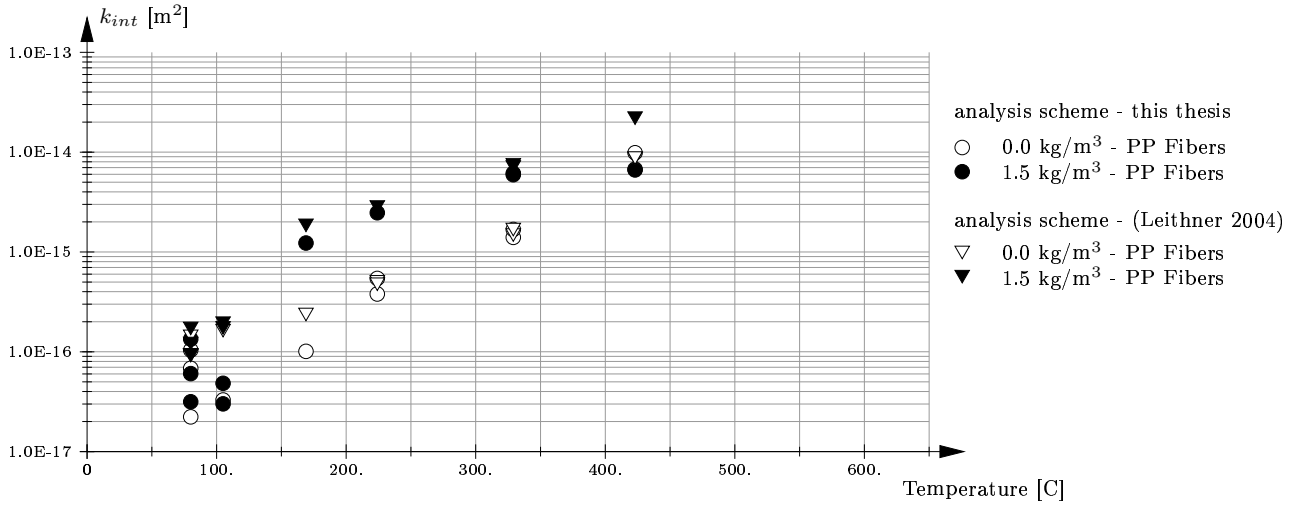

(a)

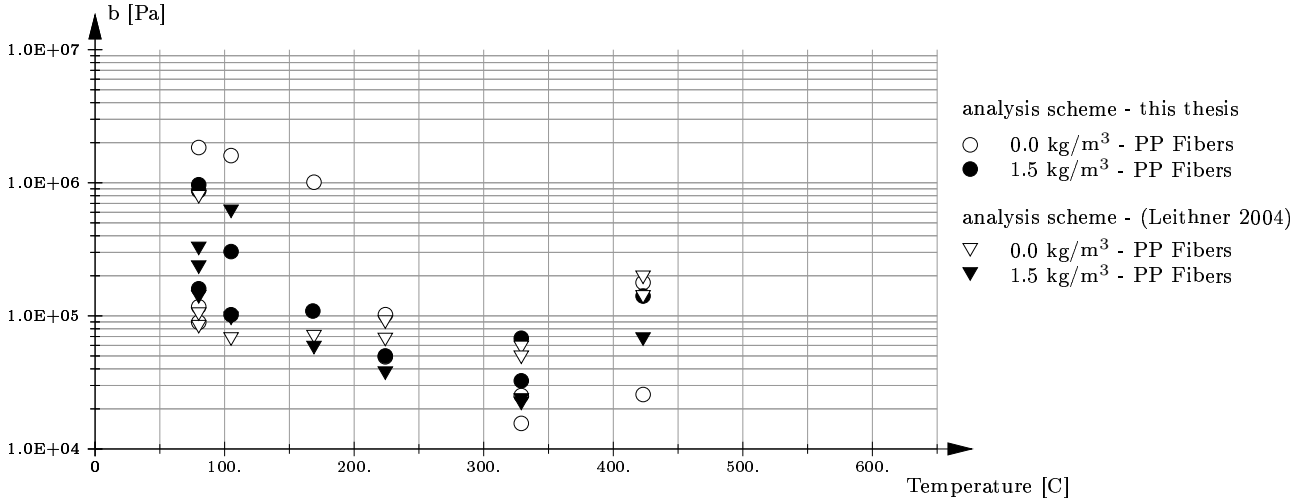

(b)

Figure 6.6: Intrinsic permeability k_{int} and parameter b obtained from two modes of analysis (test results from this thesis)

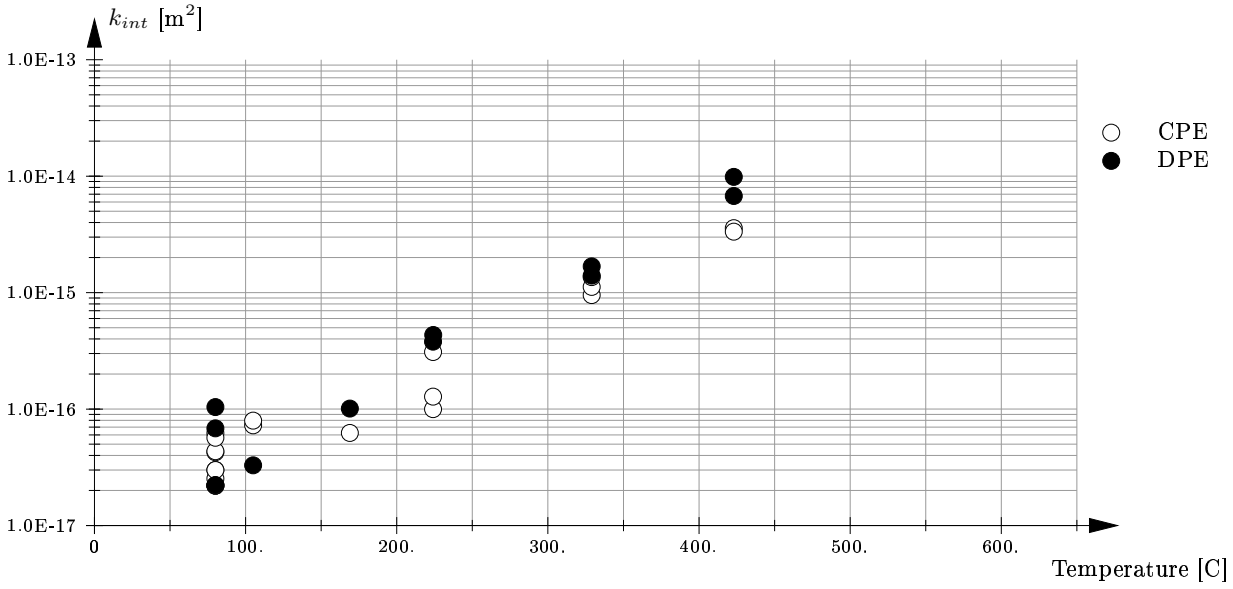

(a)

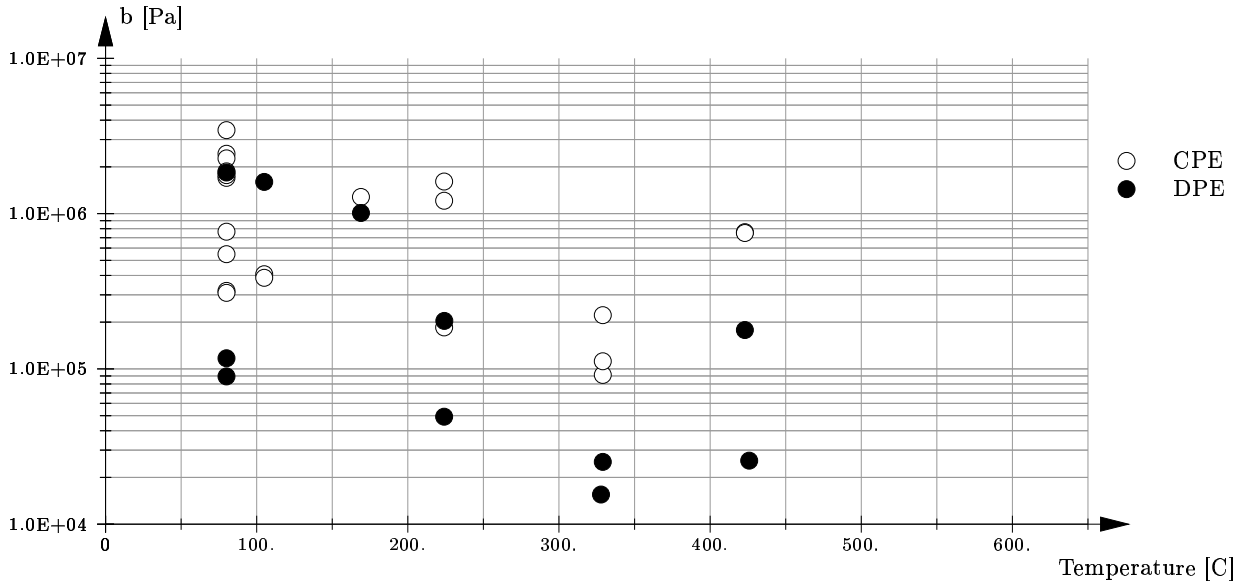

(b)

Figure 6.7: Intrinsic permeability k_{int} and parameter b for concrete without PP-fibers obtained from different types of experiments

Chapter 7

Concluding remarks

In the course of this thesis, the change of parameters, describing the permeability, with temperature of two types of concrete (with and without PP-fibers) was investigated. In contrast to the concrete investigated by Leithner (2004), the specimens were obtained from concrete blocks produced in the laboratory.

The main difference between the considered laboratory concrete and the in-situ concrete tested by Leithner (2004) results from concreting and compaction. In the laboratory, the smaller quantities of concrete are easier to compact, resulting in smaller values for k_{int} at temperatures below 105°C (see Figure 7.3). With increasing pre-heating temperature, laboratory concrete with PP-fibers gives similar values for k_{int} as in-situ concrete, characterized by a strong increase in consequence of melting of PP-fibers within $150 \leq T \leq 170$°C. The effect of melting is smaller for the in-situ concrete.

Figure 7.4 shows the parameter b with increasing pre-heating temperature. No trend of the value of b with increasing temperature is observed. As outlined in Subsection 6.2, this can be explained by the lower impact of the value of b as compared to the impact of k_{int} on the pressure distribution and, thus, on the error function minimized during the analysis scheme employed for determination of k_{int} and b.

The permeability device employed in this thesis allows conduction of both DPEs and CPEs. In contrast to the DPEs, CPEs require more time and future work should be devoted to reducing the amount of time necessary to perform CPEs. This can be reached by reducing the preparation time for the specimens to be tested, i.e., by using other sealing material than wax and silicone. The pressure regulating valves may be replaced by more accurate valves, helping to reach balance between the double-acting piston (see Figure 3.2) and the supplying pistons more quickly. Moreover, the volume of the container

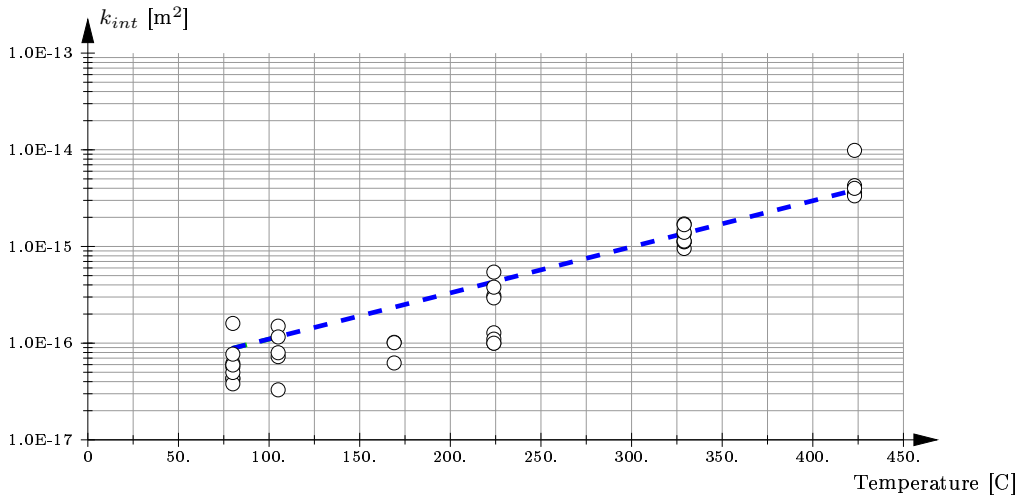

(a)

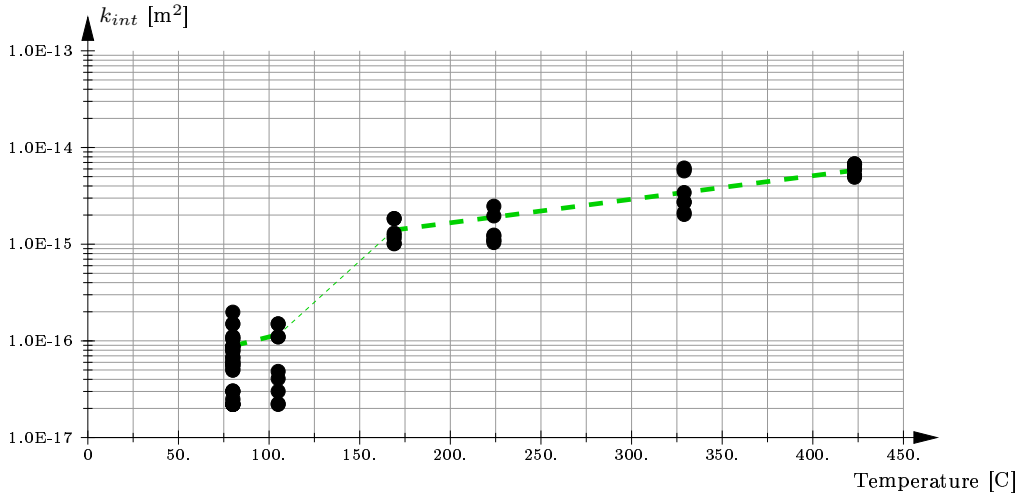

(b)

Figure 7.1: Intrinsic permeability k_{int} of laboratory concrete (a) with no and (b) with PP-fibers for different pre-heating temperatures (test results from this thesis)

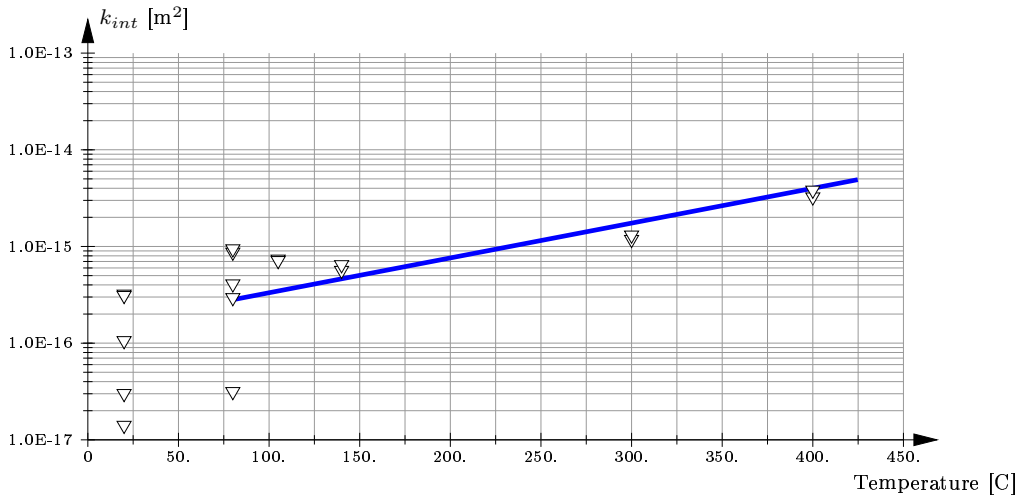

(a)

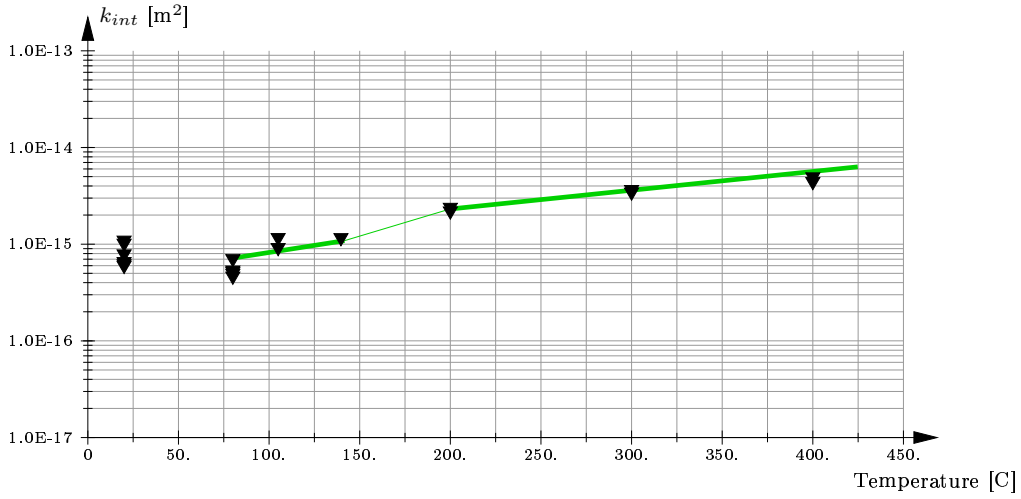

(b)

Figure 7.2: Intrinsic permeability k_{int} of in-situ concrete (a) with no and (b) with PP-fibers for different pre-heating temperatures (test results from (Leithner 2004))

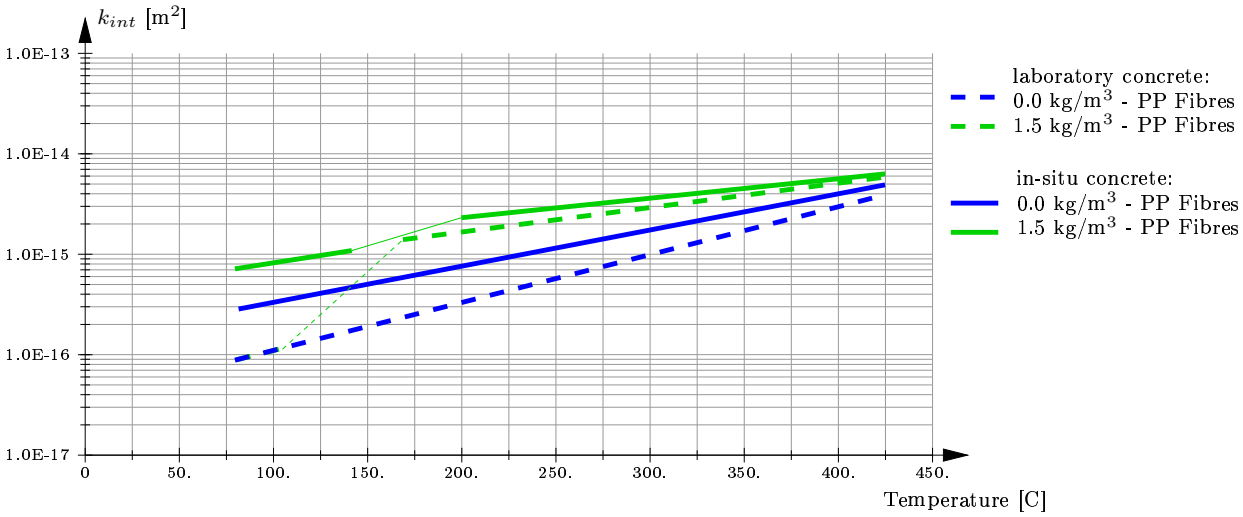

Figure 7.3: Intrinsic permeability k_{int} for two types of concrete as a function of temperature: approximations

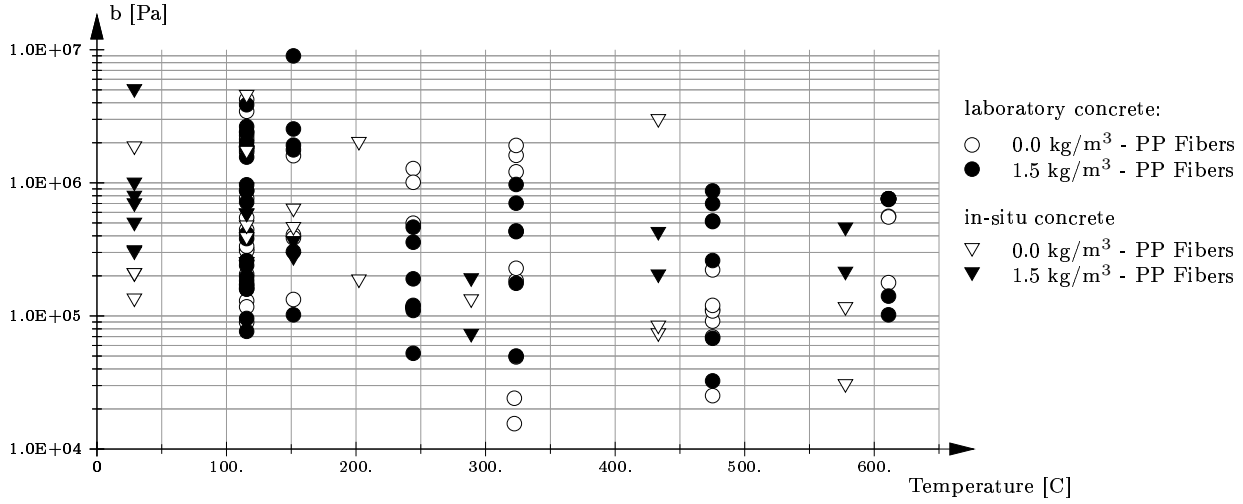

Figure 7.4: Parameter b for two types of concrete as a function of temperature

connected to the permeability device may be increased, providing a better performance of DPEs and, if also connected to the system for CPEs, less pressure variation during CPEs. Finally, the quality of the one-way valves may be improved by using more sensitive valves. All these changes in the test setup, which will be adressed in future work, may help to speed up the testing procedure, on the one hand, and to further improve the quality of the obtained results, on the other hand.

Bibliography

EC2 (1992). *Eurocode 2: Planung von Stahlbeton- und Spannbetontragwerken.* Österreichisches Normungsinstitut.

Gallé, C. and Daian, J.-F. (2000). Gas permeability of unsaturated cement-based materials: application of a multi-scale network model. *Magazine of Concrete Research*, 52(4):251–263.

Gawin, D., Pesavento, F., and Schrefler, B. A. (2002). Simulation of damage-permeability coupling in hygro-thermo-mechanical analysis of concrete at high temperatures. *Communications in Numerical Methods in Engineering*, 18(2):113–119.

Jacobs, F. (1994). *Permeabilität und Porengefüge zementgebundener Werkstoffe [Permeability and pore structure of cementitious materials].* PhD thesis, ETH Zürich, Zürich, Switzerland. In German.

Klinkenberg, L. J. (1941). The permeability of porous media to liquids and gases. *American Petroleum Institute, Drilling Production Practice*, pages 200–213.

Kusterle, W., Lindlbauer, W., Hampejs, G., Heel, A., Donauer, P.-F., Zeiml, M., Brunnsteiner, W., Dietze, R., Hermann, W., Viechtbauer, H., Schreiner, M., Vierthaler, R., Stadlober, H., Winter, H., Lemmerer, J., and Kammeringer, E. (2004). Brandbeständigkeit von Faser-, Stahl- und Spannbeton [Fire resistance of fiber-reinforced, reinforced, and prestressed concrete]. Technical Report 544, Bundesministerium für Verkehr, Innovation und Technologie, Vienna. In German.

Leithner, D. (2004). Experimental investigation of concrete subjected to fire loading: micromechanical approach for determination of the permeability. Master's thesis, Vienna University of Technology, Vienna, Austria.

Mehlhorn, G. (1996). *Der Ingenieurbau.* Oxford University Press.

Appendix A

k_{int} and b from CPEs and DPEs

Specimen	Temp. [°C]	Method	Determination of k_{int} and b according to Leithner (2004)		subsection 3.2.3	
			k_{int} [m^2]	b [Pa]	k_{int} [m^2]	b [Pa]
W0012	80	CPE-mode I	1.06E-16	1.58E+04	3.00E-17	2.43E+06
	80	CPE-mode II	1.03E-16	4.95E+04	3.80E-17	4.23E+06
	105	CPE-mode I	1.33E-16	5.85E+04	7.25E-17	4.07E+05
	105	CPE-mode II	1.60E-16	3.76E+04	1.50E-16	1.28E+07
	329	CPE-mode I	9.59E-16	1.04E+04	9.52E-16	9.15E+04
	329	CPE-mode II	1.25E-15	5.41E+04	1.12E-15	6.96E+04
	329	DPE	1.55E-15	6.01E+04	1.40E-15	2.52E+04
W0013	80	CPE-mode I	5.18E-17	2.00E+05	4.26E-17	3.18E+05
	80	CPE-mode II	5.23E-17	3.44E+05	4.97E-17	3.34E+05
	80	DPE	9.63E-17	8.13E+05	2.23E-17	1.84E+06
	224	CPE-mode I	2.79E-16	1.60E+05	1.01E-16	1.61E+06
	224	CPE-mode II	3.12E-16	1.57E+05	1.10E-16	1.23E+07
W0024	80	CPE-mode I	7.07E-17	1.17E+05	2.20E-17	1.70E+06
	80	CPE-mode II	6.77E-17	1.21E+05	5.94E-17	2.06E+05
	80	DPE	9.70E-17	8.60E+04	6.83E-17	8.94E+04
	105	CPE-mode I	1.17E-16	1.31E+05	7.96E-17	3.86E+05
	105	CPE-mode II	1.24E-16	9.87E+04	1.16E-16	1.33E+05
	105	DPE	1.71E-16	6.95E+04	3.29E-17	1.60E+06
	329	CPE-mode I	1.16E-15	8.86E+04	1.12E-15	1.12E+05
	329	CPE-mode II	1.24E-15	6.92E+04	1.23E-15	6.98E+04
	329	DPE	1.76E-15	5.07E+04	1.65E-15	1.68E+04

W0032	80	CPE-mode I	9.07E-17	1.55E+05	2.53E-17	1.77E+06
	80	CPE-mode II	8.30E-17	2.02E+05	1.60E-16	2.69E+07
	423	CPE-mode I	7.78E-15	1.76E+05	3.58E-15	7.60E+05
	423	CPE-mode II	6.85E-15	2.45E+05	4.25E-15	5.60E+05
	423	DPE	9.07E-15	2.02E+05	6.76E-15	1.78E+05
W0033	80	CPE-mode I	1.02E-16	4.18E+05	3.00E-17	3.45E+06
	80	CPE-mode II	1.03E-16	4.39E+05	1.10E-16	1.11E+07
	224	CPE-mode I	4.12E-16	7.25E+04	1.28E-16	1.21E+06
	224	CPE-mode II	3.05E-16	1.59E+05	1.00E-16	1.91E+06
	224	DPE	5.27E-16	9.31E+04	4.44E-16	1.01E+05
W0042	80	CPE-mode I	9.20E-17	9.16E+04	2.20E-17	2.27E+06
	80	CPE-mode II	9.34E-17	7.33E+04	5.82E-17	4.45E+05
W0043	80	CPE-mode I	1.05E-16	1.26E+05	6.19E-17	5.48E+05
	80	CPE-mode II	8.41E-17	2.93E+05	1.50E-16	1.65E+07
	80	DPE	1.50E-16	1.07E+05	1.04E-16	1.17E+05
	423	CPE-mode I	7.19E-15	1.37E+05	3.34E-15	7.50E+05
	423	CPE-mode II	6.53E-15	1.84E+05	3.99E-15	5.54E+05
	423	DPE	9.16E-15	1.44E+05	9.46E-15	2.87E+04
W0044	80	CPE-mode I	1.06E-16	5.13E+04	2.20E-17	1.87E+06
	80	CPE-mode II	1.12E-16	5.99E+04	8.83E-17	1.64E+05
	329	CPE-mode I	1.89E-15	6.36E+04	1.36E-15	2.22E+05
	329	CPE-mode II	1.96E-15	8.53E+04	1.71E-15	1.20E+05
W0052	80	CPE-mode I	1.13E-16	3.77E+04	4.35E-17	7.65E+05
	80	CPE-mode II	9.46E-17	9.80E+04	2.20E-17	2.13E+06
	224	CPE-mode I	4.13E-16	3.62E+04	3.09E-16	1.85E+05
	224	CPE-mode II	4.04E-16	3.92E+04	2.94E-16	2.28E+05
	224	DPE	4.99E-16	6.89E+04	3.79E-16	4.92E+04
W0054	80	CPE-mode I	8.87E-17	7.81E+04	5.67E-17	3.09E+05
	80	CPE-mode II	8.37E-17	1.23E+05	7.70E-17	1.30E+05
	169	CPE-mode I	1.83E-16	9.34E+04	6.24E-17	1.28E+06
	169	CPE-mode II	1.99E-16	6.42E+04	1.02E-16	4.98E+05
	169	DPE	2.48E-16	7.23E+04	1.01E-16	1.00E+06

Table A.1: Intrinsic permeability k and parameter b for experiments conducted in this thesis (concrete with no PP-fibers)

Specimen	Temp. [°C]	Method	Determination of k_{int} and b according to Leithner (2004)		subsection 3.2.3	
			k_{int} [m^2]	b [Pa]	k_{int} [m^2]	b [Pa]
W1512	80	CPE-mode I	8.72E-17	6.49E+04	2.21E-17	1.56E+06
	80	CPE-mode II	1.02E-16	5.33E+04	8.78E-17	9.57E+04
	105	CPE-mode I	1.13E-16	1.59E+05	2.20E-17	1.92E+06
	105	CPE-mode II	1.08E-16	1.75E+05	1.10E-16	8.99E+06
	105	DPE	1.82E-16	6.33E+05	4.84E-17	1.23E+06
	329	CPE-mode I	5.43E-15	4.93E+04	2.12E-15	6.99E+05
	329	CPE-mode II	5.49E-15	3.59E+04	3.42E-15	2.61E+06
W1514	80	CPE-mode I	1.06E-16	7.54E+04	2.20E-17	2.39E+06
	80	CPE-mode II	1.19E-16	4.30E+04	1.05E-16	7.66E+04
	169	CPE-mode I	2.05E-15	2.07E+04	1.84E-15	5.24E+04
	169	CPE-mode II	1.90E-15	3.98E+04	1.56E-15	1.20E+05
W1522	80	CPE-mode I	1.11E-16	1.30E+05	5.00E-17	8.74E+05
	80	CPE-mode II	9.78E-17	1.85E+05	8.43E-17	2.40E+05
	224	CPE-mode I	2.65E-15	1.27E+04	1.24E-15	4.30E+05
	224	CPE-mode II	2.49E-15	1.64E+04	1.21E-15	4.35E+05
W1523	80	CPE-mode I	1.40E-16	2.29E+05	3.04E-17	3.86E+06
	80	CPE-mode II	1.11E-16	3.73E+05	1.10E-16	1.22E+07
	80	DPE	1.80E-16	2.41E+05	1.34E-16	2.11E+05
	423	CPE-mode I	9.87E-15	3.10E+05	6.78E-15	1.02E+05
	423	CPE-mode II	1.26E-14	2.04E+05	6.61E-15	7.61E+05
	423	DPE	2.30E-14	6.94E+04	6.64E-15	8.02E+05
W1524	80	CPE-mode I	9.91E-17	4.59E+04	5.61E-17	3.81E+05
	80	CPE-mode II	9.79E-17	1.48E+04	1.50E-16	1.73E+07
	105	CPE-mode I	1.24E-16	2.24E+05	4.07E-17	1.77E+06
	105	CPE-mode II	1.15E-16	2.28E+05	1.10E-16	1.03E+07
	105	DPE	2.03E-16	9.95E+04	3.01E-17	3.10E+06
	329	CPE-mode I	5.61E-15	2.93E+04	2.03E-15	8.70E+05
	329	CPE-mode II	5.40E-15	5.40E+04	2.72E-15	5.17E+05
	329	DPE	7.82E-15	2.42E+04	5.98E-15	2.01E+04
W1532	80	CPE-mode I	4.86E-17	6.44E+05	2.20E-17	1.86E+06
	80	CPE-mode II	5.67E-17	6.73E+05	5.32E-17	7.15E+05
	224	CPE-mode I	2.28E-15	3.63E+04	1.10E-15	7.04E+05

	224	CPE-mode II	2.28E-15	2.63E+04	1.10E-15	1.20E+04
	224	DPE	2.96E-15	3.85E+04	2.47E-15	1.01E+05
W1533	423	CPE-mode I	1.24E-14	9.11E+04	5.20E-15	7.57E+05
	423	CPE-mode II	1.24E-14	6.64E+04	4.93E-15	7.54E+05
W1543	80	CPE-mode I	6.12E-17	1.59E+05	5.60E-17	2.61E+05
	80	CPE-mode II	7.29E-17	1.03E+05	6.64E-17	1.59E+05
	169	CPE-mode I	1.53E-15	4.06E+04	1.15E-15	1.90E+05
	169	CPE-mode II	1.43E-15	5.39E+04	1.30E-15	1.10E+05
W1544	80	CPE-mode I	9.34E-17	1.31E+04	2.44E-17	2.03E+06
	80	CPE-mode II	9.81E-17	1.44E+04	6.73E-17	4.14E+05
	80	DPE	1.27E-16	1.44E+05	3.16E-17	2.42E+06
	224	CPE-mode I	2.63E-15	2.71E+04	1.96E-15	1.76E+05
	224	CPE-mode II	2.88E-15	5.51E+04	1.04E-15	6.07E+05
W1552	80	CPE-mode I	8.23E-17	1.79E+05	7.98E-17	1.97E+05
	80	CPE-mode II	8.26E-17	1.62E+05	7.96E-17	1.84E+05
	169	CPE-mode I	1.71E-15	2.00E+04	1.02E-15	3.58E+05
	169	CPE-mode II	1.57E-15	2.94E+04	1.01E-15	4.65E+05
	169	DPE	1.94E-15	5.99E+04	1.23E-15	1.09E+05
W1553	80	CPE-mode I	8.22E-17	2.07E+05	8.73E-17	1.71E+05
	80	CPE-mode II	8.80E-17	1.64E+05	8.69E-17	1.73E+05
	105	CPE-mode I	8.30E-17	3.85E+05	2.24E-17	2.54E+06
	105	CPE-mode II	8.11E-17	3.91E+05	1.50E-16	1.49E+07
	329	CPE-mode I	5.06E-15	8.86E+04	2.73E-15	5.12E+05
	329	CPE-mode II	5.40E-15	3.82E+04	5.73E-15	1.13E+04
	329	DPE	7.45E-15	2.28E+04	5.94E-15	1.10E+06
W1554	80	CPE-mode I	7.70E-17	2.60E+05	3.01E-17	2.65E+06
	80	CPE-mode II	3.99E-18	1.24E+05	1.98E-16	2.78E+07
	80	DPE	9.78E-17	3.33E+05	6.04E-17	5.97E+05
	423	CPE-mode I	1.24E-14	9.30E+04	5.92E-15	7.60E+05
	423	CPE-mode II	1.25E-14	1.27E+05	5.97E-15	7.60E+05

Table A.2: Intrinsic permeability k and parameter b for experiments conducted in this thesis (concrete with PP-fibers)

Specimen	Temp. [°C]	Method	Determination of k_{int} and b according to Leithner (2004)		subsection 3.2.3	
			k_{int} [m^2]	b [Pa]	k_{int} [m^2]	b [Pa]
of11	20	DPE	4.13E-16	3.08E+05	3.21E-16	4.12E+05
	140	DPE	8.01E-16	9.47E+04	5.65E-16	1.89E+05
of12	20	DPE	1.21E-16	1.50E+05	1.06E-16	2.11E+05
	200	DPE	1.26E-15	3.51E+04	8.58E-16	1.34E+05
of13	80	DPE	1.37E-17	4.94E+06	3.15E-17	1.79E+06
	400	DPE	7.61E-15	1.29E+05	3.25E-15	7.20E+05
of21	20	DPE	3.26E-17	5.55E+05	1.41E-17	1.74E+06
	300	DPE	1.22E-15	6.02E+04	1.18E-15	7.00E+04
of22	20	DPE	1.37E-16	4.65E+06	3.11E-16	1.89E+06
	105	DPE	1.00E-15	6.48E+05	7.39E-16	8.52E+05
of31	20	DPE	2.20E-17	5.99E+04	8.00E-18	8.81E+05
	600	DPE	3.53E-14	2.49E+05	9.79E-15	1.76E+06
of32	20	DPE	4.60E-17	7.88E+04	3.01E-17	3.21E+05
	400	DPE	3.50E-15	5.44E+04	3.75E-15	1.74E+04
of33	300	DPE	1.25E-15	4.73E+04	1.31E-15	3.17E+04
of41	80	DPE	6.87E-16	2.21E+06	4.09E-16	3.50E+06
of42	80	DPE	7.42E-16	1.35E+06	8.71E-16	9.73E+05
	140	DPE	1.58E-16	9.45E+06	6.47E-16	1.87E+06
of51	80	DPE	5.22E-16	3.83E+05	2.95E-16	7.81E+05
	105	DPE	1.79E-15	1.37E+05	7.14E-16	6.47E+05
of52	80	DPE	7.54E-16	2.45E+06	9.44E-16	1.67E+06

Table A.3: Intrinsic permeability k and parameter b for experiments reported in (Leithner 2004) (concrete with no PP-fibers)

Specimen	Temp. [°C]	Method	Determination of k_{int} and b according to Leithner (2004)		Determination of k_{int} and b according to subsection 3.2.3	
			k_{int} [m^2]	b [Pa]	k_{int} [m^2]	b [Pa]
mf11	20	DPE	3.60E-16	3.73E+06	6.26E-16	1.82E+06
mf12	20	DPE	1.07E-15	4.53E+05	1.02E-15	4.86E+05
	200	DPE	4.36E-15	1.04E+05	2.40E-15	3.51E+05
mf13	80	DPE	1.15E-15	3.07E+05	7.08E-16	5.89E+05
	400	DPE	8.10E-15	2.62E+05	4.44E-15	7.60E+05
mf21	20	DPE	1.45E-15	4.64E+05	7.93E-16	9.42E+05
	300	DPE	3.80E-15	7.18E+05	3.45E-15	7.51E+05
mf22	20	DPE	1.33E-15	1.68E+05	1.10E-15	2.62E+05
	105	DPE	1.81E-15	1.89E+05	1.17E-15	3.67E+05
mf23	80	DPE	7.45E-16	1.13E+05	4.99E-16	2.43E+05
	600	DPE	1.55E-14	1.47E+06	9.49E-15	2.72E+06
mf31	20	DPE	3.94E-16	2.09E+06	6.60E-16	1.01E+06
mf32	20	DPE	5.63E-16	7.75E+05	6.03E-16	7.01E+05
	400	DPE	5.23E-15	6.82E+05	4.96E-15	7.60E+05
mf33	80	DPE	1.44E-15	2.10E+05	4.66E-16	1.07E+06
	105	DPE	1.24E-15	1.77E+05	9.22E-16	2.75E+05
mf34	80	DPE	7.72E-16	2.36E+05	4.84E-16	4.77E+05
	140	DPE	1.71E-15	1.97E+05	1.26E-15	2.92E+05
mf41	80	DPE	7.61E-16	1.76E+05	5.22E-16	3.15E+05
	200	DPE	4.39E-15	5.50E+04	2.20E-15	3.60E+05
mf42	80	DPE	6.66E-16	2.05E+05	5.39E-16	2.64E+05
	300	DPE	5.22E-15	3.20E+05	3.67E-15	5.60E+05
mf43	140	DPE	5.59E-16	1.99E+05	4.14E-16	2.97E+05

Table A.4: Intrinsic permeability k and parameter b for experiments reported in (Leithner 2004) (concrete with PP-fibers)